Journal of Geotechnical and Geoenvironmental Engineering
https://doi.org/10.1061/JGGEFK.GTENG-10195
This is an accepted manuscript. It may differ from the final version:

A New One-Dimensional Thermal Elastic Visco–plastic Model for the Thermal Creep of Saturated Clayey Soils

Ze-Jian Chen (corresponding author)
Postdoctoral Fellow, Department of Civil and Environmental Engineering, The Hong Kong Polytechnic University, Hong Kong SAR, China
ORCID ID: 0000-0001-7855-6234
Email: zejchen@polyu.edu.hk

and

Jian-Hua Yin
Chair Professor of Soil Mechanics, Department of Civil and Environmental Engineering, The Hong Kong Polytechnic University, Hong Kong SAR, China
ORCID ID: 0000-0002-7200-3695
Email: cejhyin@polyu.edu.hk

Abstract: Temperature significantly affects the mechanical properties of geomaterials, particularly the creep behavior of soft clayey soils. Thus, an appropriate constitutive model to describe the time-dependent stress–strain behavior of clayey soils at various temperatures is necessary. This study performed temperature-controlled oedometer tests on two clayey soils: the Hong Kong marine deposit (HKMD) and kaolinite clay. The thermally-induced strain and creep strain rates under different temperature paths were investigated and discussed. A novel one-dimensional (1D) thermal elastic visco–plastic (TEVP) model was developed based on Yin and Graham's 1D elastic visco–plastic (EVP) model. In the proposed model, the visco–plastic strain rate of soils can be described using three state variables: effective stress, strain, and temperature. The proposed model can be implemented in creep analysis conveniently with the equivalent time concept. The prediction results of the TEVP model were consistent with the experimental data for HKMD and kaolin.

Keywords: temperature, clayey soils, oedometer, creep, thermal elastic visco–plastic (TEVP) model

1 Introduction

Temperature effects are seldom considered in conventional geotechnical engineering. However, in many engineering applications, such as heated submarine pipelines (Rawat and Agarwal, 1982; Scheeiner et al., 2006; Wen et al., 2010; Thusyanthan et al., 2011; Shahrokhabadi et al., 2020), deep disposal of radioactive waste (Houston et al., 1985; Graham et al., 2001; Abuel-Naga et al., 2007; Cui et al., 2009; Kurz et al., 2016), exploitation of geothermal resources (Dupray et al., 2014; Li et al., 2018; Laloui and Sutman, 2020; Bergström et al., 2021), and accelerated consolidation of soft clayey soils with thermal vertical drains (Abuel-Naga et al., 2006a; Wang J. et al., 2020), temperature significantly affects the hydro-mechanical behavior of clayey soils. The increase in temperature in clayey soils could induce excessive or differential settlements, increase excess pore water pressure, and change soil strength, endangering the corresponding facilities. There are also concerns about the influences of different temperatures between in situ and laboratory conditions on measuring soil parameters for engineering design (Graham et al., 2001).

In recent years, laboratory investigations have been conducted on the thermo-mechanical properties of clayey soils. It has been widely observed that increasing the temperature causes volumetric strain and increases the excess pore water pressure of clayey soils in laboratory and field tests (Houston et al., 1985; Abuel-Naga et al., 2007a; Bergström et al., 2021). The thermally-induced strain is compressive, large, and irreversible-dominated for normally consolidated soils but small and reversible-dominated for over-consolidated soils (Modaressi and Laloui, 1997; Burghignoli et al., 2000; Neaupane et al., 2005; Abuel-Naga et al., 2007a,b; Coccia and McCartney, 2016a, b). It was also found that the yielding stress of clayey soils decreased as the temperature increased in oedometer and constant-rate-of-strain consolidation tests (Akagi and Komiya, 1995; Tsutsumi and Tanaka, 2012; Abuel-Naga et al., 2006b; Jarad, 2016). The effects of temperature on the creep behavior of clayey soils have also been observed and reported in several experimental studies (Houston et al., 1985; Fox and Edil, 1996; Zhu and Qi, 2018). Based on thermal cycling tests on reconstituted clay, Burghignoli et al. (2000) concluded that the creep behavior of clayey soils was dependent on their recent temperature history. Cui et al. (2009) performed high-pressure consolidation tests on stiff Boom clay samples at different temperatures and found that the rate of strain was dependent on the temperature. Some studies suggested that the secondary consolidation coefficient C_α increases with temperature (Jarad, 2016; Zhu and Qi, 2018; Kaddouri et al., 2019), whereas others obtained different results at lower temperatures (Li et al., 2018). In summary, the time-dependent stress–strain behavior of clayey soils is closely related to temperature and stress history; however, there still lacks a widely accepted theoretical framework for describing the thermal creep characteristics of clayey soils.

Several attempts have been made to model the stress–strain behavior of clayey soils with consideration of temperature effects. Zhou et al. (1998) developed a thermoporoelastic model to simulate thermal consolidation, considering only elastic deformation. Other researchers proposed several thermal elastic–plastic (TEP) models based on the framework of the Cam-Clay model (Abuel-Naga et al., 2009; Cekerevac et al., 2002; Graham et al., 2001; Hueckel and Baldi, 1990; Laloui and Cekerevac, 2003). To consider time dependency, Laloui et al. (2008) developed a thermal visco–plastic model to describe temperature- and rate-dependent yielding stresses. Zhu and Qi (2018) adopted the power function originally proposed by Moritz (1995) to describe the temperature- and rate-dependent yielding stress of structured soils. The variation in the creep coefficient with the temperature was also considered. Wang et al. (2020) adopted Moritz’s (1995) power function to model the thermal visco–plastic behavior of clayey soils under triaxial conditions. Coccia and McCartney (2016a, b) developed a thermally-enhanced creep model for poorly drained soils by considering a temperature-dependent creep coefficient.

However, the thermal elastic viscoplastic (TEVP) model of clayey soils can still be improved. Many existing models are based on correlations between temperature and pre-consolidation pressure. Owing to the uncertain nature of soils, the pre-consolidation pressure measured from parallel isothermal compression tests may suffer from indistinct trends, and repetition may be required (Tidfors and Sällfors, 1989; Eriksson, 1992). Meanwhile, the thermal elastic behavior was not considered in many thermal visco–plastic models (Laloui et al., 2008; Zhu and Qi, 2018). In addition, a systematic and consistent understanding of the creep behavior of clayey soils under various temperature histories still needs to be established. These considerations emphasize the importance of developing a new TEVP model to describe the thermal creep behavior of clayey soils.

2 Findings from temperature-controlled oedometer tests

2.1 Test apparatus, materials, and procedure

A special oedometer cell was set up to investigate the stress–strain behavior of clayey soils under different thermal paths. The test apparatus consisted of a conventional oedometer and temperature control systems with an electric heating wire, a temperature sensor, and a thermostat. The heating wire was installed around the confining ring of the specimen, and the temperature sensor was placed in the middle of the surrounding water in the oedometer cell. The heating system can control the temperature in the cell from 20 °C to 60 °C with an error within ± 0.2 °C. Fig. 1 shows the details of the test setup.

Preliminary tests were performed to calibrate the apparatus. A trial soil specimen was installed in the apparatus and several temperature sensors were inserted at different positions to examine the uniformity of the temperature distribution within the soil. The trial soil specimens were subjected to different temperatures. Fig. 2(a) shows that the temperature measured at different distances from the center of the soil specimen was uniform (variation within ± 0.5) and approximately 1–2 °C lower than the temperature in water at 40 °C and 60 °C. Therefore, the temperatures were set at 42 °C and 62 °C on the thermostat for 40 °C and 60 °C in the soil, respectively, during the oedometer tests. Fig. 2(b) shows the measured temperature with time for different heating and cooling stages, indicating that the temperature in the soil could be balanced within 1 h. From 20 to 40 °C, the balance time was less than 30 min. The thermal deformation of the test apparatus components (e.g., porous stones, stainless steel cap and base, and loading piston) at different temperatures was 0.0009 mm/°C, obtained by performing heating–cooling tests without the existence of soil specimens. The deformation was considered elastic and excluded from the calculation of the soil strain.

Two materials were used in this study. One was the Hong Kong marine deposit (HKMD), primarily composed of silt and approximately 20 % of clay (particles with a diameter less than 2 μm), and kaolinite clay (kaolin), comprising approximately 77 % of clay. Fig. 3 shows the particle size distribution curves for the two soils. Table 1 lists the liquid limit, plastic limit, and specific gravity of the two soils.

The soils were reconstituted in a slurry state. The initial water contents were 100 % and 120 % for the HKMD and kaolin (approximately twice the liquid limit), respectively. The slurry was poured into a steel cylinder with a diameter of 110 mm and consolidated under vertical loading by dead weight. The maximum consolidation pressure for the reconstitution was approximately 20 kPa. All loads were removed after the end of primary consolidation. A confining ring (ϕ 70 mm $\times H$ 19 mm) was used to prepare the oedometer specimens from the cylinder.

Oedometer tests were performed under multistage loading and step-change temperatures. Three targeted temperatures of 20 °C, 40 °C, and 60 °C (293 K, 313 K, and 333 K) were applied to the soils under different loading stages, as shown in Table 2. The test was designed to investigate the one-dimensional (1D) time-dependent stress–strain behavior of clayey soils under different temperature and stress paths. The results indicate that the primary consolidation was completed within 100 min using Casagrande's logarithm-of-time fitting method for all loading stages. The measured temperature inside the oedometer also stabilized during this period. To investigate the creep behavior, the value of t_0 in Yin and Graham's (1989, 1994)'s 1D EVP model was set to 100 min in this study. The vertical strain occurring after 100 min of loading was considered as "pure creep" under constant effective stress and temperature. The complicated thermo–hydro–mechanical process within t_0 can be neglected.

2.2 Characteristics of thermally-induced strains with time

As shown in Table 2, staged changes in temperature were applied to soils at 100 kPa and 400 kPa; the corresponding vertical strains are plotted against time in Fig. 4 and 5, respectively. Under heating, an additional compressive strain was induced, and creep accelerated rapidly. The reduction in the viscosity of pore water at higher temperatures transforms bound water into free water, generating additional consolidation and causing heating-induced compression. The decrease in water viscosity also reduces some interparticle friction and gaps, resulting in local collapse, contraction, and reorganization of the soil skeleton.

As shown in Fig. 4, there is no clear turning point exhibiting the "end of primary consolidation" (EOP) during heating, as typically observed under incremental mechanical loading. This trend is similar to the test results for Boom clay obtained by Cui et al. (2009). Although the pore pressure was not measured, it can still be assumed that the dissipation of the thermally-induced excess pore pressure was completed rapidly. This is because the strain increment under thermal loading is much smaller than that under mechanical loading; therefore, the consolidation speed of the thermal loading stages should be faster than that of the mechanical loading stages, according to Terzaghi's 1D consolidation theory. In addition, heating accelerates the consolidation process by increasing permeability (Houston et al., 1987; Towhata et al., 1993; Delage et al., 2000; Abuel-Naga et al., 2005; Jarad et al., 2019). Based on these considerations, the strain occurring after 100 min of temperature change can certainly be regarded as "pure creep" under constant temperature and effective stress. Fig. 4 demonstrates that the creep curve after 100 min of heating is a straight line, and is similar to that induced by mechanical loading at normal temperature (i.e., 20 °C).

Figs. 5(a)–(d) show the vertical strain due to temperature changes with time for the HKMD and kaolin under 100 kPa and 400 kPa, respectively. The first heating contributed to a large compression strain. The soil experienced minimal volumetric strain during the cooling process, with small strain rates. The vertical strain and strain rate increased after reheating. This indicates that the amount and rate of thermally-induced strain are closely related to the temperature history of clayey soils.

2.3 Characteristic of strain–temperature relations under heating and cooling

Fig. 6 shows the strain–temperature ($\varepsilon_z - \ln T$) curves of the HKMD and kaolin under heating–cooling cycles at different constant vertical stress. The data were collected at t_0 (100 min) after the loading or temperature changes, guaranteeing the total dissipation of excess pore water pressure and temperature equilibrium.

Fig. 6 shows that the slopes of the $\varepsilon_z - \ln T$ curves during the first heating (virgin heating) and cooling–reheating differed significantly. The soil experienced a larger volumetric contraction under virgin heating. This volume strain was unrecoverable during the subsequent cooling process. The variation in strain during cooling–reheating was smaller and showed a reversible (elastic) trend. This reversible strain can be positive (compressive) or negative (expansive) according to the fitted trendlines. The reversible deformation of the soil under temperature changes can be attributed to the thermal expansion and contraction of soil particles and water and other reversible deformations of the soil skeleton.

The characteristics shown in Fig. 6 strongly suggest that the temperature–strain relations are highly similar to the stress–strain relations for clayey soils. The virgin heating process is similar to normal compression, whereas the cooling–reheating process shares similarities with the unloading–reloading process.

2.4 Correlations between creep strain rate, strain, and temperature

The creep strain rate (i.e., visco–plastic strain rate) is essential for modeling the visco–plastic behavior of soils. The creep strain rate $\dot{\varepsilon}_{z,i}^{vp}$ at time t_i can be calculated as the averaged secant slope on the $\varepsilon_z - t$ curves from the oedometer tests, as shown in Fig. 7 and Eq. (1).

$$\dot{\varepsilon}_{z,i}^{vp} = \left.\frac{\partial \varepsilon_z^{vp}}{\partial t}\right|_i \approx \frac{1}{2}\left(\frac{\varepsilon_{z,i-1}^{vp} - \varepsilon_{z,i}^{vp}}{t_{i-1} - t_i} + \frac{\varepsilon_{z,i+1}^{vp} - \varepsilon_{z,i}^{vp}}{t_{i+1} - t_i}\right) \tag{1}$$

where i represents the current point of time, $i-1$ and $i+1$ are neighboring points before and after i, respectively, and ε_z^{vp} is the vertical creep strain.

According to the 1D EVP model of Yin and Graham (1989, 1994), the creep strain rate of clayey soils depends on the current stress and strain states, as shown in Eq. (2).

$$\dot{\varepsilon}_z^{vp} = \frac{\psi}{Vt_0} \cdot \exp\left[-\frac{V}{\psi}\left(\varepsilon_z - \varepsilon_{zp0}\right)\right] \cdot \left(\frac{\sigma_z^{'}}{\sigma_{zp0}^{'}}\right)^{\frac{\lambda}{\psi}} \tag{2}$$

where $\dot{\varepsilon}_z^{vp}$ is the creep strain rate, $V = 1 + e_0$ is the initial specific volume, ψ is the creep coefficient, t_0 is the reference time, λ is the normal compression index obtained at t_0, $\sigma_{zp0}^{'}$ is the reference pre-consolidation pressure, and ε_{zp0} is the strain measured at t_0 under $\sigma_{zp0}^{'}$. $\left(\sigma_{zp0}^{'}, \varepsilon_{zp0}\right)$ is a fixed point in the reference time line. Eq. (2) can be rewritten as

$$\ln \dot{\varepsilon}_z^{vp} = \ln \frac{\psi}{Vt_0} + \left[-\frac{V}{\psi}\left(\varepsilon_z - \varepsilon_{zp0}\right)\right] + \frac{\lambda}{\psi}\ln\left(\frac{\sigma_z^{'}}{\sigma_{zp0}^{'}}\right) \tag{3}$$

According to Eq. (3), $\ln \dot{\varepsilon}_z^{vp}$ and ε_z follow a linear relation under constant $\sigma_z^{'}$.

Fig. 8 shows the calculated creep strain rate $\dot{\varepsilon}_z^{vp}$ against vertical strain ε_z at different temperatures T and vertical stress $\sigma_z^{'}$. $\ln \dot{\varepsilon}_z^{vp}$ and ε_z are linearly correlated under constant T and $\sigma_z^{'}$, indicating the effectiveness of Eq. (3) under different constant temperatures. Regardless of the temperature paths, the data points with the same temperature fall on the same $\ln \dot{\varepsilon}_z^{vp} - \varepsilon_z$ line. However, the $\ln \dot{\varepsilon}_z^{vp} - \varepsilon_z$ lines under different temperatures deviate from each other in a nearly parallel pattern. Therefore, Eq. (3) should be modified to

$$\ln \dot{\varepsilon}_z^{vp} = \ln \frac{\psi}{Vt_0} + \left[-\frac{V}{\psi}\left(\varepsilon_z - \varepsilon_{zp0}\right) \right] + \frac{\lambda}{\psi} \ln \left(\frac{\sigma_z^{'}}{\sigma_{zp0}^{'}} \right) + f\left(T\right) \quad (4a)$$

$$\Rightarrow \dot{\varepsilon}_z^{vp} = \frac{\psi}{Vt_0} \exp\left[-\frac{V}{\psi}\left(\varepsilon_z - \varepsilon_{zp0}\right) \right] \left(\frac{\sigma_z^{'}}{\sigma_{zp0}^{'}} \right)^{\frac{\lambda}{\psi}} \cdot g\left(T\right) \quad (4b)$$

where $f\left(T\right)$ and $g\left(T\right)$ are unknown functions of temperature derived in the succeeding sections.

In addition, Fig. 8 shows that $\dot{\varepsilon}_z^{vp}$ increases instantly with heating and decreases with cooling. This also indicates the similarity between the thermal and stress effects on clayey soils as the creep strain rate increases with loading and decreases with unloading according to the EVP models (Yin and Graham, 1994; Chen et al., 2021).

The creep behavior is typically considered to be related to the viscous interparticle contact with the diffusion double layer and the viscous flow of the adsorbed pore fluid (Le et al., 2012). Therefore, the micro-origin of the heating-dependent creep strain rate could be attributed to the heating-induced reduction in the viscosity of the double-layer water and the energy barrier of adsorbed water (Brochard et al., 2017). However, to verify these hypotheses, more quantified molecular dynamics simulations need to be performed in the future.

2.5 Compression curves under stage-changed temperatures

Fig. 9(a) shows the compression curves ($\varepsilon_z - \ln \sigma_z^{'}$) from 50 kPa to 800 kPa for the two soils under different temperatures in the normal compression state. The strain for each stage was measured at $t_0 = 100$ min after loading increments. The dashed lines represent the normal compression lines (NCL) at 20 °C, obtained by connecting the stress–strain points at three loading stages (50 kPa, 100 kPa, and 400 kPa). According to the $\varepsilon_z - \ln \sigma_z^{'}$ curves, the stress–strain points at 40 °C and 60 °C (under 200 kPa and 800 kPa, respectively) were below the NCLs at 20 °C. The higher the temperature, the lower the position of the data point. However, as shown in Fig. 5 and 8, the temperature effects on the $\varepsilon_z - \ln\sigma_z^{'}$ curves were less significant than on creep, owing to the relatively lower viscosity of the HKMD and kaolin. In previous studies, the temperature effects on the curves were significant for some clays with higher clay content and viscosity (Abuel-Naga et al. 2006; Tsutsumi and Tanaka 2012; Jarad et al. 2017). Fig. 9(b) shows the $\varepsilon_z - \ln\sigma_z^{'}$ curves of the two representative marine clays under temperature changes. Natural Bangkok clay was reported by Abuel-Naga et al. (2006), whereas the results for natural HK clay were obtained from an additional oedometer test performed by the authors. For these two clays, the thermally-induced strain was much larger.

Although the thermal effects on the $\varepsilon_z - \ln\sigma_z^{'}$ curves are less apparent for the two soils, the thermal creep effects are still significant, particularly for long-term engineering design. These results also imply the difficulty of accurately determining the yielding stress from the $\varepsilon_z - \ln\sigma_z^{'}$ curves for previous TEVP models (e.g., Laloui et al. 2008, Zhu and Qi 2018, Wang et al. 2020), and alternative models need to be established.

3 Development of the 1D thermal elastic visco–plastic (TEVP) model for clayey soils

3.1 Introduction to Yin and Graham's 1D EVP model

Under the 1D strain condition, the conventional elastic–plastic stress–strain relationship of clayey soils can be expressed as

$$\varepsilon_z = \begin{cases} \varepsilon_{z0} + \dfrac{\kappa}{V}\ln\dfrac{\sigma_z^{'}}{\sigma_{z0}^{'}} & \text{at over-consolidation state} \\ \varepsilon_{z0} + \dfrac{\kappa}{V}\ln\dfrac{\sigma_{zp}^{'}}{\sigma_{z0}^{'}} + \dfrac{\lambda}{V}\ln\dfrac{\sigma_z^{'}}{\sigma_{zp}^{'}} = \varepsilon_{zp} + \dfrac{\lambda}{V}\ln\dfrac{\sigma_z^{'}}{\sigma_{zp}^{'}} & \text{at normal consolidation state} \end{cases} \quad (5)$$

where $\sigma_{zp}^{'}$ is the apparent pre-consolidation pressure, ε_{zp} is the strain under $\sigma_{zp}^{'}$, κ is the elastic recompression index for unloading-reloading, and λ is the compression index for normal compression.

In the 1D EVP model by Yin and Graham (1989, 1994), the normal compression line measured at a fixed time of t_0 is redefined as the "reference time line," whereas the unloading–reloading line is redefined as the "instant time line". The strain along the instant time line is considered elastic, whereas the strain along the reference time line contains visco–plastic deformation. A series of "equivalent time lines" can be drawn approximately parallel to the reference time line to account for time-dependent compression, as shown in Eq. (6):

$$\varepsilon_z = \varepsilon_{zp0} + \frac{\lambda}{V}\ln\frac{\sigma_z^{'}}{\sigma_{zp0}^{'}} + \frac{\psi}{V}\ln\frac{t_e + t_0}{t_0} \quad (6)$$

where t_e is the equivalent time describing the distance between the current stress–strain point and the reference time line, ψ is the creep coefficient, and $\left(\sigma_{zp0}^{'}, \varepsilon_{zp0}\right)$ is a fixed point at the reference time line fitted from the oedometer test data.

One hypothesis adopted in Yin and Graham's model and other similar isotach EVP models (Suklje, 1957; Leroueil et al., 1985; Yin et al., 2010) is that the visco–plastic strain rate $\dot{\varepsilon}_z^{vp}$ is dependent only on the current stress–strain state but is irrelevant to the stress history. From Eq. (6), t_e and $\dot{\varepsilon}_z^{vp}$ are expressed in the following path-independent form:

$$t_e = \exp\left[\left(\varepsilon_z - \varepsilon_{zp0} - \frac{\lambda}{V}\ln\frac{\sigma_z^{'}}{\sigma_{zp0}^{'}}\right)\frac{V}{\psi}\right]t_0 - t_0 \tag{7a}$$

$$\dot{\varepsilon}_z^{vp} = \frac{\psi}{V}\frac{1}{t_e + t_0} = \frac{\psi}{Vt_0}\exp\left[-\frac{V}{\psi}\left(\varepsilon_z - \varepsilon_{zp0}\right)\right]\left(\frac{\sigma_z^{'}}{\sigma_{zp0}^{'}}\right)^{\frac{\lambda}{\psi}} \tag{7b}$$

3.2 Modeling the thermally-induced strain

According to the experimental results, the thermally-induced volumetric strain consists of two parts: a reversible (elastic) part and an irreversible (viscoplastic) part. Because the thermally-induced strain exhibits high similarity with the stress-induced strain, it would be convenient to model the temperature–strain behaviour in a way similar to classical stress–strain models. First, the thermally-induced elastic strain $\Delta\varepsilon_z^{Te}$ under a temperature change from T_0 to T can be described using the following nonlinear function:

$$\Delta\varepsilon_z^{Te} = \frac{\kappa_T}{V}\ln\frac{T}{T_0} \tag{8}$$

where T is the temperature in Kelvin (K), T_0 is a reference temperature (e.g., 293 K), and κ_T is the "cooling and reheating" index describing the thermal elastic behavior. $\Delta\varepsilon_z^{Te}$ is an instant and reversible strain under temperature changes because of the elastic thermal expansion/contraction of pore water and soil particles and other reversible deformations of the soil skeleton. $\Delta\varepsilon_z^{Te}$ is considered to be independent of the over-consolidation ratio (OCR). Eq. (8) is equivalent to the nonlinear formula $d\varepsilon_v^{Te} = \alpha\frac{dT}{T}$ defined by Abuel-Naga et al. (2007b) to describe the elastic volume changes of clay, where $\alpha = \frac{\kappa_T}{V}$.

The thermally-induced viscoplastic strain is dominant in the virgin heating stage, with similar behavior to the stress-induced viscoplastic strain in the normal compression state. Following the expression $\Delta\varepsilon_z = \frac{\lambda}{V}\ln\frac{\sigma_z^{'}}{\sigma_{zp0}^{'}}$ for the normal compression line, a "virgin heating line" can be defined as

$$\Delta\varepsilon_z^T = \frac{\lambda_T}{V}\ln\frac{T}{T_0} \tag{9}$$

where λ_T is the virgin heating compression index describing the relationship between the thermally-induced strain $\Delta\varepsilon_z^T$ and the temperature during virgin heating.

Because $\Delta\varepsilon_z^T$ is time-dependent owing to creep, as found in the oedometer tests, the virgin heating line should be obtained at a specific reference time. The reference time should be selected after balancing the temperature inside the soil sample and total dissipation of excess pore pressure, suggested to be the same as t_0 in the EVP model. In this study, the reference time t_0 = 100 min was considered reasonable for the HKMD and kaolin, as discussed in previous sections. Creep compression ε_z^{vp} after t_0 under virgin heating is similar to that under normal compression, expressed as $\varepsilon_z^{vp} = \frac{\psi}{V}\ln\frac{t_e + t_0}{t_0}$.

Fig. 10 shows a schematic of the virgin heating line, cooling–reheating line, and equivalent time lines for clayey soils under constant effective stress. For point A at the reference time line, where the soil is normally consolidated under a reference temperature (e.g., room temperature of 20 °C), the equivalent time is $t_e = 0$. The soil then creeps as t_e increases and becomes over-consolidated (from A to A'). After heating from T_0 to a new temperature, the equivalent time decreases and $\dot{\varepsilon}_z^{vp}$ increases as the soil approaches the virgin heating line (from A' to B), where t_e

is zero. If the soil is suddenly cooled, t_e increases rapidly and $\dot{\varepsilon}_z^{vp}$ decreases. If the soil is reheated and reapproaches the virgin heating, t_e decreases, and $\dot{\varepsilon}_z^{vp}$ increases again. Thus, the heating process reduces t_e and increases $\dot{\varepsilon}_z^{vp}$, whereas the cooling process causes the opposite. This mechanism coincides with the experimental observations presented in previous sections. However, it should be noted that the proposed model was developed based on experimental observations within a temperature range of 20 °C to 60 °C.

3.3 Modeling the visco–plastic strain rate in stress–strain–temperature space

As shown in Fig. 11, the vertical strain under any stress and temperature (e.g., point B' in Fig. 11) can be described using the normal compression, virgin heating, and equivalent timelines, as indicated in Eq. (10):

$$\varepsilon_z = \varepsilon_{zp0} + \frac{\lambda}{V}\ln\frac{\sigma'_z}{\sigma'_{zp0}} + \frac{\lambda_T}{V}\ln\frac{T}{T_0} + \frac{\psi}{V}\ln\frac{t_e+t_0}{t_0} \tag{10}$$

where σ'_{zp0} and ε_{zp0} are fixed parameters measured under T_0. It should be noted that κ_T, λ_T and ψ can be temperature-dependent, whereas λ and κ are reported to be less relevant to temperature (Fox and Edil, 1996; Crilly, 1996; Abuel-Naga et al., 2009; Batenipour et al., 2009; Kurz et al., 2016; Kaddouri et al., 2019). Using Eq. (10), t_e and $\dot{\varepsilon}_z^{vp}$ should be expressed as

$$t_e = \exp\left[\left(\varepsilon_z - \varepsilon_{zp0} - \frac{\lambda}{V}\ln\frac{\sigma'_z}{\sigma'_{zp0}} - \frac{\lambda_T}{V}\ln\frac{T}{T_0}\right)\frac{V}{\psi}\right]t_0 - t_0 \tag{11a}$$

$$\dot{\varepsilon}_z^{vp} = \frac{\psi}{V}\frac{1}{t_e+t_0} = \frac{\psi}{Vt_0} \cdot \exp\left[-\frac{V}{\psi}\left(\varepsilon_z - \varepsilon_{zp0}\right)\right] \cdot \left(\frac{\sigma'_z}{\sigma'_{zp0}}\right)^{\frac{\lambda}{\psi}} \cdot \left(\frac{T}{T_0}\right)^{\frac{\lambda_T}{\psi}} \tag{11b}$$

According to Eq. (11b), the 1D visco–plastic strain rate $\dot{\varepsilon}_z^{vp}$ of a clayey soil is dependent on three field variables (strain ε_z, effective stress $\sigma_z^{'}$, and temperature T) but independent of the paths of these variables. The visco–plastic strain rate can also be uniquely described using equivalent time t_e. Other parameters, such as ψ, $\sigma_{zp0}^{'}$, and ε_{zp0}, are measurable in conventional or isothermal oedometer tests under constant temperature *T*. This model is a simple extension of Yin and Graham's 1D EVP model. Using Eq. (11b), the preassumed functions in Eq. (4) can be solved as

$$g(T)=\left(\frac{T}{T_0}\right)^{\frac{\lambda_T}{\psi}} \tag{12a}$$

$$f(T)=\frac{\lambda_T}{\psi}\ln\left(\frac{T}{T_0}\right) \tag{12b}$$

Eq. (11) introduces a set of temperature-dependent equivalent time lines below or above the reference time line, as shown in Fig. 11. The equivalent time and visco–plastic strain rate change with temperature, which induces different amount of creep deformation per unit time.

Fig. 12 further reveals the elastic visco–plastic behavior of clayey soils in the strain, stress, and temperature spaces. The equivalent time lines are extended to inclined "equivalent time planes" in the $\varepsilon_z-\ln\sigma_z^{'}-\ln T$ space using Eq. (11). The intersections of equivalent time planes and an equal-temperature plane correspond to the conventional equivalent time lines in Yin and Graham's 1D EVP model. The intersections of equivalent time planes and an equal-stress plane become the equivalent time lines in Fig.10. A zero-equivalent-time plane passes through the reference time line at T_0. For a soil element at any state of $\left(\sigma_z^{'},\varepsilon_z,T\right)$, an increase in either temperature or effective stress will increase the visco–plastic strain rate. By contrast, a decrease in either temperature or effective stress will reduce the visco–plastic strain rate. It should be noted that the equivalent time planes can be curved surfaces if λ, ψ, and λ_T are not constant at different stress or temperatures, although test results on Bangkok clay show that the value of λ_T may be independent of vertical effective stress (Abuel-Naga et al., 2007a).

3.4 Comparisons with previous works

The proposed model can be used to explain the stress history-dependent thermal behavior of soils, as reported by previous researchers (Modaressi and Laloui, 1997; Burghignoli et al., 2000; Neaupane et al., 2005; Abuel-Naga et al., 2007a,b; Cui et al., 2009). When soil is heavily over-consolidated (by unloading, long-term creep, or cooling), the equivalent time is large, and the thermally-induced strain is almost reversible, primarily controlled by $\frac{\kappa_T}{V}$. When soil is normally consolidated (with zero equivalent time), a significant irreversible viscoplastic strain is induced during heating (primarily controlled by $\frac{\lambda_T}{V}$ and $\frac{\psi}{V}$).

The proposed model shares some similarities with previous models in that the apparent pre-consolidation pressure $\sigma_{zp}^{'}$ (i.e., yielding stress) is a temperature- and time-dependent variable (Hueckel and Borsetto, 1990; Laloui and Cekerevac, 2003; Abuel-Naga et al., 2007b; Laloui et al., 2008; Zhu and Qi, 2018; Wang et al., 2020). The equivalent time lines are similar to the isotach. The intersection between the current equivalent time line and the initial instant corresponds to the yielding stress $\sigma_{zp}^{'}$ under a specific loading rate. Therefore, the following expressions are obtained by substituting $\varepsilon_z = \varepsilon_{zp0} + \frac{\kappa}{V}\ln\frac{\sigma_{zp}^{'}}{\sigma_{zp0}^{'}} + \frac{\lambda}{V}\ln\frac{\sigma_z^{'}}{\sigma_{zp}^{'}}$ into Eq. (11b):

$$\dot{\varepsilon}_z^{vp} = \frac{\psi}{Vt_0} \cdot \exp\left[\left(-\frac{\kappa}{\psi}\ln\frac{\sigma'_{zp}}{\sigma'_{zp0}} - \frac{\lambda}{\psi}\ln\frac{\sigma'_z}{\sigma'_{zp}}\right)\right] \cdot \left(\frac{\sigma'_z}{\sigma'_{zp0}}\right)^{\frac{\lambda}{\psi}} \cdot \left(\frac{T}{T_0}\right)^{\frac{\lambda_T}{\psi}} \tag{13a}$$

$$\Rightarrow \sigma'_{zp} = \sigma'_{zp0}\left(\dot{\varepsilon}_z^{vp}\frac{Vt_0}{\psi}\right)^{\frac{\psi}{\lambda-\kappa}}\left(\frac{T}{T_0}\right)^{-\frac{\lambda_T}{\lambda-\kappa}} \tag{13b}$$

where σ'_{zp} is the yielding stress for the current temperature and strain rate in the 1D condition, and ε_{zp} is the corresponding vertical strain. According to Eq. (13b), the yielding stress decreases with an increase in temperature, which is consistent with most existing models (Laloui et al., 2008; Zhu and Qi, 2018; Wang et al., 2020).

The expressions in Eq. (13) require σ'_{zp} to be measured on a logarithmic scale, which may rely on a graphic method and may be affected by manual or intersample errors. Determining κ_T and λ_T from the oedometer tests in this study will be more convenient and requires fewer repeated tests. Moreover, with the equivalent time $t_e\left(\sigma'_z, \varepsilon_z, T\right)$, the model can be easily implemented in either numerical simulations or handy calculations for soil deformations under complicated thermomechanical conditions.

4 Verifications of the TEVP model with test data

4.1 Calibration of parameters

Performing a staged heating oedometer test for normally consolidated soil is the most convenient method for determining the parameters κ_T and λ_T. Thermally-induced strains should be measured using a predefined t_0. Virgin heating tests can be used for fitting $\frac{\lambda_T}{V}$, whereas a cooling–reheating test can be used for fitting $\frac{\kappa_T}{V}$. Fig. 13(a) shows the results of the heating tests (from 20 °C to 40 °C to 60 °C) for kaolin under 1600 kPa; each temperature was sustained for 100 min without long-term creep. The value of $\frac{\lambda_T}{V}$ was calculated as 0.044, as shown in Fig. 13(b).

However, in other loading stages, heating was performed on the soils after a long creep time. Therefore, the soil state may not be able to return to the virgin heating line after heating. Therefore, the fitted $\frac{\lambda_T}{V}$ in Fig. 6 may be inaccurate. Another method is proposed for fitting $\frac{\lambda_T}{V}$ using the $\dot{\varepsilon}_z^{vp} - \varepsilon_z$ curves shown in Fig. 8. The differences in vertical strain under equal $\dot{\varepsilon}_z^{vp}$ between different temperatures, as shown in Fig. 14, should be measured carefully and used to calculate $\frac{\lambda_T}{V}$ with the following equations:

$$\frac{\psi}{Vt_0}\exp\left[-\frac{V}{\psi}\left(\varepsilon_{z1}-\varepsilon_{zp}\right)\right]\left(\frac{\sigma_z^{'}}{\sigma_{zp}^{'}}\right)^{\frac{\lambda}{\psi}}\left(\frac{T_1}{T_0}\right)^{\frac{\lambda_T}{\psi}}=\frac{\psi}{Vt_0}\exp\left[-\frac{V}{\psi}\left(\varepsilon_{z2}-\varepsilon_{zp}\right)\right]\left(\frac{\sigma_z^{'}}{\sigma_{zp}^{'}}\right)^{\frac{\lambda}{\psi}}\left(\frac{T_2}{T_0}\right)^{\frac{\lambda_T}{\psi}} \quad (14a)$$

$$\Rightarrow \frac{\lambda_T}{V}=\frac{\varepsilon_{z1}-\varepsilon_{z2}}{\ln\left(T_1/T_2\right)} \quad (14b)$$

where $\Delta\varepsilon_{z1}$ and $\Delta\varepsilon_{z1}$ are the measured strains under T_1 and T_2 with equal $\dot{\varepsilon}_z^{vp}$. Using Eq. (14b), the values of $\frac{\lambda_T}{V}$ are calculated at different vertical effective stress, as shown in Table 3. It can be observed that the value of $\frac{\lambda_T}{V}$ for kaolin under 1600 kPa from the first method is similar to the values from the second method under different stresses.

According to the proposed TEVP model, $\frac{\kappa_T}{V}$ is the slope of the thermal elastic deformation and thus can be determined from a cooling test under an over-consolidated state, where the time-dependent deformation is small. As shown in Fig. 6, $\frac{\kappa_T}{V}$ fitted at a normal consolidation or slightly over-consolidation state can be positive or negative, and the absolute value is much smaller than that of $\frac{\lambda_T}{V}$. Fig. 15 shows the thermally-induced deformation of soils in different OCRs (representing only the ratio of the historical maximum effective stress over current effective stress) by unloading from 400 kPa. It can be observed that time-dependent swelling strain occurs and is much larger for OCR=6 than for OCR=1.5. Swelling is another time-dependent behavior during unloading (Yin and Tong, 2011, Feng et al., 2016), which was not discussed in this study. According to Feng et al. (2017), OCR=1.5 is likely to be in the neutral region between the creep and swelling sides, and the deformation should be almost purely elastic. For simplification, $\frac{\kappa_T}{V}$ is considered constant for all stress–strain states and fitted from the cooling process when OCR=1.5 and $\sigma_z^{'}$=267 kPa.

The values of $\frac{\kappa}{V}$, $\frac{\lambda}{V}$, and $\frac{\psi}{V}$ can be determined through multistage oedometer tests. In this model, $\frac{\kappa}{V}$ can be obtained from the unloading curves in the multistage oedometer tests under a constant temperature, and $\frac{\lambda}{V}$ can be fitted by the normal compression line under $T_0 = 20\ ^{\circ}\mathrm{C} = 293\mathrm{K}$ and t_0. $\frac{\psi}{V}$ was fitted using creep tests under a constant temperature. Because no strong evidence shows the temperature or stress dependency of $\frac{\psi}{V}$ under different loadings, it is assumed that $\frac{\psi}{V}$ is constant for the tested soils.

4.2 Predicted creep compression by TEVP compared with test results

With the proposed model and calibrated parameters, time-dependent compression curves of the HKMD and kaolin at different temperatures were constructed. Immediate thermal elastic strains occur with changes in temperature under constant vertical stress. The thermally-induced excess pore pressure should be fully dissipated within $t_0 = 100$ min for the tested soils. Therefore, the new volumetric strain at t_0 after changing the temperature from T_1 to T_2 is determined as

$$\varepsilon_{z2}^{t_0} = \max\left[\left(\varepsilon_{z1} + \frac{\kappa_T}{V}\ln\frac{T_2}{T_1}\right), \left(\varepsilon_{zp0} + \frac{\lambda}{V}\ln\frac{\sigma_z^{'}}{\sigma_{zp0}^{'}} + \frac{\lambda_T}{V}\ln\frac{T_2}{T_0}\right)\right] \tag{15}$$

where ε_{z1} is the vertical strain before the temperature change, and $\varepsilon_{z2}^{t_0}$ is the vertical strain at t_0 under the new temperature. The equivalent time t_{e2} of the specimen after t_0 at the new temperature can be calculated according to Eq. (11a) as

$$t_{e2} = \exp\left[\left(\varepsilon_{z2}^{t_0} - \varepsilon_{zp0} - \frac{\lambda}{V}\ln\frac{\sigma_z^{'}}{\sigma_{zp0}^{'}} - \frac{\lambda_T}{V}\ln\frac{T}{T_0}\right)\frac{V}{\psi}\right]t_0 - t_0 \tag{16a}$$

If t_{e2} is equal to zero, then the soil state is on the virgin heating line. If t_{e2} is greater than zero, the soil state is below the virgin heating line. The vertical strain $\varepsilon_{z2}(t)$ with elapsed time under the new temperature can then be calculated as

$$\varepsilon_{z2}(t) = \varepsilon_{z2}^{t_0} + \frac{\psi}{V}\ln\frac{t_{e2}+t}{t_{e2}+t_0} \quad \text{for } t > 100 \text{ min} \tag{16b}$$

Fig. 16 shows the predicted and measured strain–time curves of the HKMD and kaolin owing to temperature changes under different constant vertical stresses. The curves predicted by the TEVP model fit well with the test data, confirming the reliability of the model. The evolution of t_e with time and temperature is also shown in the figure, indicating that heating always reduces the equivalent time, whereas cooling results in the opposite.

5 Conclusions

This study performed temperature-controlled oedometer tests to investigate the creep behavior of two clayey soils under different temperature conditions. Based on experimental observations, a new 1D TEVP model is proposed to describe the thermal creep behavior of saturated clayey soils. The TEVP model was extended from Yin and Graham's (1989, 1994) 1D EVP model with equivalent time, and the temperature was introduced as a state variable. Thermal elastic and thermal visco–plastic deformations were considered in the model with two independent parameters: κ_T and λ_T. The following conclusions were drawn:

(1) The effects of temperature on the time-dependent behavior of clayey soils were similar to the effects of mechanical loading. Virgin heating, cooling, and reheating have different effects on the 1D compression of soils. Temperature conditions significantly influence the creep behavior of clayey soils.

(2) The visco–plastic strain rate $\dot{\varepsilon}_z^{vp}$ is dependent on the current state of the effective stress, temperature, and strain, but is independent of the history of these variables. The equivalent timelines in Yin and Graham's EVP model can be extended to inclined equivalent time planes in the stress–strain–temperature space. Each equivalent time plane uniquely

represents the viscoplastic strain rate $\dot{\varepsilon}_z^{vp}$. The concept of equivalent time enables the convenient modeling of creep in soils with complicated temperature and stress histories.

(3) The proposed TEVP model was calibrated and validated using experimental data. The results indicate that the proposed model can simulate the thermal creep behavior of two clayey soils accurately.

Further studies need to be carried out to determine the temperature and stress dependency of Ψ, κ_T, and λ_T, to demonstrate the correlations between the proposed parameters with basic properties of soil such as plasticity index, and to validate the model with a wider range of temperatures as in natural conditions (e.g., from 0 °C to 100 °C or even higher). Different test methods, such as constant-rate-of-strain, stress relaxation, laboratory model, and field tests, should also be performed to verify the effectiveness of the proposed model under more general conditions.

Data Availability Statement

Some or all data, models, or code that support the findings of this study are available from the corresponding author upon reasonable request.

Acknowledgement

The work in this paper is supported by a Research Impact Fund (RIF) project (R5037-18) and three GRF projects (PolyU 152179/18E; PolyU 152130/19E; PolyU 152100/20E) from Research Grants Council (RGC) of Hong Kong Special Administrative Region Government of China. The authors also acknowledge the financial supports from Research Institute for Sustainable Urban Development of The Hong Kong Polytechnic University and a grant (ZDBS) from The Hong Kong Polytechnic University.

References

Abuel-Naga, H. M., Bergado, D. T., Soralump, S., & Rujivipat, P. (2005). Thermal consolidation of soft Bangkok clay. *Lowland Technology International*, *7*(1, June), 13-21.

Abuel-Naga, H. M., Bergado, D. T., & Chaiprakaikeow, S. (2006a). Innovative thermal technique for enhancing the performance of prefabricated vertical drain during the preloading process. *Geotextiles and Geomembranes*, *24*(6), 359-370. https://doi.org/10.1016/j.geotexmem.2006.04.003

Abuel-Naga, H. M., Bergado, D. T., Ramana, G. V., Grino, L., Rujivipat, P., & Thet, Y. (2006b). Experimental evaluation of engineering behavior of soft Bangkok clay under elevated temperature. *Journal of geotechnical and geoenvironmental engineering*, *132*(7), 902-910. https://doi.org/10.1061/(asce)1090-0241(2006)132:7(902)

Abuel-Naga, H. M., Bergado, D. T., & Bouazza, A. (2007a). Thermally induced volume change and excess pore water pressure of soft Bangkok clay. *Engineering Geology*, *89*(1-2), 144-154. https://doi.org/10.1016/j.enggeo.2006.10.002

Abuel-Naga, H. M., Bergado, D. T., Bouazza, A., & Ramana, G. V. (2007b). Volume change behaviour of saturated clays under drained heating conditions: experimental results and constitutive modeling. *Canadian Geotechnical Journal*, *44*(8), 942-956. https://doi.org/10.1139/T07-031

Abuel-Naga, H. M., Bergado, D. T., Bouazza, A., & Pender, M. (2009). Thermomechanical model for saturated clays. *Géotechnique*, *59*(3), 273-278. https://doi.org/10.1680/geot.2009.59.3.273

Akagi, H., & Komiya, K. (1995). Constant rate of strain consolidation properties of clayey soil at high temperature. In *Proc. Int. Symp. Compression and Consolidation of Clayey Soils–IS–Hiroshima* (Vol. 95, pp. 3-8).

Bergström, A., Javed, S., & Dijkstra, J. (2021). Field test of a floating thermal pile in sensitive clay. *Géotechnique*, *71*(4), 334-345. https://doi.org/10.1680/jgeot.19.P.094

Brochard, L., Honório, T., Vandamme, M., Bornert, M., & Peigney, M. (2017). Nanoscale origin of the thermo-mechanical behavior of clays. *Acta Geotechnica*, *12*(6), 1261-1279. https://doi.org/10.1007/s11440-017-0596-3

Burghignoli, A., Desideri, A., & Miliziano, S. (2000). A laboratory study on the thermomechanical behaviour of clayey soils. *Canadian Geotechnical Journal*, *37*(4), 764-780.

Cekerevac, C., Laloui, L., & Vulliet, L. (2002). Dependency law for thermal evolution of preconsolidation pressure. In *Proceedings of the 8th International Symposium on Numerical Models in Geomechanics, Rome, Italy, Edited by GN Pande and S. Pietruszczak. AA Balkema* (pp. 687-692).

Coccia, C. J. R., & McCartney, J. S. (2016). Thermal volume change of poorly draining soils I: Critical assessment of volume change mechanisms. *Computers and Geotechnics*, *80*, 26-40. https://doi.org/10.1016/j.compgeo.2016.06.009

Coccia, C. J. R., & McCartney, J. S. (2016). Thermal volume change of poorly draining soils II: model development and experimental validation. *Computers and Geotechnics*, *80*, 16-25. https://doi.org/10.1016/j.compgeo.2016.06.010

Crilly, T.N. 1996. Unload–reload tests on saturated illite specimens at elevated temperatures. M.Sc. thesis, University of Manitoba, Winnipeg, Man.

Cui, Y. J., Le, T. T., Tang, A. M., Delage, P., & Li, X. L. (2009). Investigating the time-dependent behaviour of Boom clay under thermomechanical loading. *Géotechnique*, *59*(4), 319-329. https://doi.org/10.1680/geot.2009.59.4.319

Delage, P., Sultan, N., & Cui, Y. J. (2000). On the thermal consolidation of Boom clay. *Canadian Geotechnical Journal*, *37*(2), 343-354. https://doi.org/10.1139/t99-105

Dupray, F., Laloui, L., & Kazangba, A. (2014). Numerical analysis of seasonal heat storage in an energy pile foundation. *Computers and Geotechnics*, *55*, 67-77. https://doi.org/10.1016/j.compgeo.2013.08.004

Eriksson, L. G. (1992). Compression properties of sulphide soils–Influence from time and temperature, a laboratory study. *Licentiate thesis, Luleå University of Technology, Luleå [In Swedish]*.

Feng, W. Q., Lalit, B., Yin, Z. Y., & Yin, J. H. (2017). Long-term non-linear creep and swelling behavior of Hong Kong marine deposits in oedometer condition. *Computers and Geotechnics*, *84*, 1-15. https://doi.org/10.1016/j.compgeo.2016.11.009

Fox, P. J., & Edil, T. B. (1996). Effects of stress and temperature on secondary compression of peat. *Canadian Geotechnical Journal*, *33*(3), 405-415.

Graham, J., Tanaka, N., Crilly, T., & Alfaro, M. (2001). Modified Cam-Clay modelling of temperature effects in clays. *Canadian geotechnical journal*, *38*(3), 608-621. https://doi.org/10.1139/cgj-38-3-608

Houston, S. L., Houston, W. N., & Williams, N. D. (1985). Thermo-mechanical behavior of seafloor sediments. *Journal of Geotechnical Engineering*, *111*(11), 1249-1263. https://doi.org/10.1680/jgeot.19.P.094

Houston, S. L., & Lin, H. D. (1987). A thermal consolidation model for pelagic clays. *Marine Georesources & Geotechnology*, *7*(2), 79-98. https://doi.org/10.1080/10641198709388209

Hueckel, T., & Baldi, G. (1990). Thermoplasticity of saturated clays: experimental constitutive study. *Journal of geotechnical engineering*, *116*(12), 1778-1796.

Jarad, N. (2016). *Temperature impact on the consolidation and creep behaviour of compacted clayey soils* (Doctoral dissertation, Université de Lorraine). https://doi.org/10.1080/19648189.2017.1311806

Jarad, N., Cuisinier, O., & Masrouri, F. (2019). Effect of temperature and strain rate on the consolidation behaviour of compacted clayey soils. *European Journal of Environmental and Civil Engineering*, *23*(7), 789-806. https://doi.org/10.1080/19648189.2017.1311806

Kaddouri, Z., Cuisinier, O., & Masrouri, F. (2019). Influence of effective stress and temperature on the creep behavior of a saturated compacted clayey soil. *Geomechanics for Energy and the Environment*, *17*, 106-114. https://doi.org/10.1016/j.gete.2018.09.002

Kuntiwattanakul, P., Towhata, I., Ohishi, K., & Seko, I. (1995). Temperature effects on undrained shear characteristics of clay. *Soils and Foundations*, *35*(1), 147-162.

Kurz, D., Sharma, J., Alfaro, M., & Graham, J. (2016). Semi-empirical elastic–thermoviscoplastic model for clay. *Canadian Geotechnical Journal*, *53*(10), 1583-1599. https://doi.org/10.1139/cgj-2015-0598

Laloui, L., & Cekerevac, C. (2003). Thermo-plasticity of clays: an isotropic yield mechanism. *Computers and Geotechnics*, *30*(8), 649-660. https://doi.org/10.1016/j.compgeo.2003.09.001

Laloui, L., Leroueil, S., & Chalindar, S. (2008). Modelling the combined effect of strain rate and temperature on one-dimensional compression of soils. *Canadian Geotechnical Journal*, *45*(12), 1765-1777. https://doi.org/10.1139/T08-093

Laloui, L., & Sutman, M. (2020). Experimental investigation of energy piles: From laboratory to field testing. *Geomechanics for Energy and the Environment*, 100214. https://doi.org/10.1016/j.gete.2020.100214

Le, T. M., Fatahi, B., & Khabbaz, H. (2012). Viscous behaviour of soft clay and inducing factors. *Geotechnical and Geological Engineering*, *30*(5), 1069-1083. https://doi.org/10.1007/s10706-012-9535-0

Leroueil, S., Kabbaj, M., Tavenas, F., & Bouchard, R. (1985). Stress–strain–strain rate relation for the compressibility of sensitive natural clays. *Géotechnique*, *35*(2), 159-180. https://doi.org/10.1680/geot.1985.35.2.159

Li, Y., Dijkstra, J., & Karstunen, M. (2018). Thermomechanical creep in sensitive clays. *Journal of Geotechnical and Geoenvironmental Engineering*, *144*(11), 04018085. https://doi.org/10.1061/(ASCE)GT.1943-5606.0001965

Modaressi, H., & Laloui, L. (1997). A thermo- viscoplastic constitutive model for clays. *International journal for numerical and analytical methods in geomechanics*, *21*(5), 313-335. https://doi.org/10.1002/(SICI)1096-9853(199705)21:5<313::AID-NAG872>3.0.CO;2-5

Neaupane, K. M., Nanakorn, P., Sirayapivat, O., & Kanborirak, S. (2006). Effects of temperature on 1-D consolidation characteristics of clayey soil. In *Proceedings of the 16th International Conference on Soil Mechanics and Geotechnical Engineering, Osaka, Japan, 12-16 September, 2005* (pp. 417-420). Millpress Science Publishers.

Rawat, P. C., & Agarwal, S. L. (1982). Determination of thermal conductivity of soils: A need for computing heat loss through buried submarine pipelines. *Society of Petroleum Engineers Journal*, *22*(04), 558-562.

Scheiner, S., Pichler, B., Hellmich, C., & Eberhardsteiner, J. (2006). Loading of soil-covered oil and gas pipelines due to adverse soil settlements–Protection against thermal dilatation-induced wear, involving geosynthetics. *Computers and Geotechnics*, *33*(8), 371-380. https://doi.org/10.1016/j.compgeo.2006.08.003

Shahrokhabadi, S., Cao, T. D., & Vahedifard, F. (2020). Thermal Effects on Hydromechanical Response of Seabed-Supporting Hydrocarbon Pipelines. *International Journal of Geomechanics*, *20*(1), 04019143. https://doi.org/10.1061/(ASCE)GM.1943-5622.0001534

Suklje, L. (1957). The analysis of the consolidation process by the isotaches method. In *Proc. 4th ICSMFE* (Vol. 1, pp. 200-206).

Tanaka, N., Graham, J., & Lingnau, B. E. (1995). A thermal elastic plastic model based on Modified Cam Clay. In *Proceedings of the 10th Panamerican Conference on Soil Mechanics and Foundations Engineering, Guadalajara, Mexico* (Vol. 1, pp. 252-263).

Thusyanthan, N. I., Cleverly, W., Haigh, S. K., & Ratnam, S. (2011, February). Thermal imaging, thermal conductivity of soil and heat loss from buried pipelines. In *The Offshore Pipeline Technology Conference, Amsterdam*.

Tidfors, M., & Sällfors, G. (1989). Temperature effect on preconsolidation pressure. *Geotechnical Testing Journal*, *12*(1), 93-97. https://doi.org/10.1520/GTJ10679J

Towhata, I., Kuntiwattanaku, P., Seko, I., & Ohishi, K. (1993). Volume change of clays induced by heating as observed in consolidation tests. *Soils and Foundations*, *33*(4), 170-183. https://doi.org/10.3208/sandf1972.33.4_170

Tsutsumi, A., & Tanaka, H. (2012). Combined effects of strain rate and temperature on consolidation behavior of clayey soils. *Soils and Foundations*, *52*(2), 207-215. https://doi.org/10.1016/j.sandf.2012.02.001

Wang, J., Cai, Y., Yuan, G., Fu, H., Sun, W., Hu, X., ... & Ni, J. (2020). Temperature effects on dredged slurry performance under vacuum preloading. *Canadian Geotechnical Journal*, *57*(12), 1970-1981. https://doi.org/10.1139/cgj-2019-0272

Wang, K., Wang, L., & Hong, Y. (2020). Modelling thermo-elastic–viscoplastic behaviour of marine clay. *Acta Geotechnica*, 1-17. https://doi.org/10.1007/s11440-020-00917-9

Wen, Z., Sheng, Y., Jin, H., Li, S., Li, G., & Niu, Y. (2010). Thermal elasto-plastic computation model for a buried oil pipeline in frozen ground. *Cold Regions Science and Technology*, *64*(3), 248-255. https://doi.org/10.1016/j.coldregions.2010.01.009

Yin, J. H., & Graham, J. (1989). Viscous–elastic–plastic modelling of one-dimensional time-dependent behaviour of clays. *Canadian geotechnical journal*, *26*(2), 199-209.

Yin, J. H., & Graham, J. (1994). Equivalent times and one-dimensional elastic viscoplastic modelling of time-dependent stress–strain behaviour of clays. *Canadian Geotechnical Journal*, *31*(1), 42-52. https://doi.org/10.1139/t94-005

Yin, J. H., & Graham, J. (1996). Elastic visco-plastic modelling of one-dimensional consolidation. *Geotechnique*, *46*(3), 515-527. https://doi.org/10.1680/geot.1996.46.3.515

Yin, Z. Y., Chang, C. S., Karstunen, M., & Hicher, P. Y. (2010). An anisotropic elastic–viscoplastic model for soft clays. *International Journal of Solids and Structures*, *47*(5), 665-677. https://doi.org/10.1016/j.ijsolstr.2009.11.004

Yin, J. H., & Tong, F. (2011). Constitutive modeling of time-dependent stress–strain behaviour of saturated soils exhibiting both creep and swelling. *Canadian Geotechnical Journal*, *48*(12), 1870-1885. https://doi.org/10.1139/t11-076

Zhu, Q. Y., & Qi, P. (2018). Numerical Modeling of Thermal-Dependent Creep Behavior of Soft Clays under One-Dimensional Condition. *Advances in Civil Engineering*, *2018*. https://doi.org/10.1155/2018/9827673

Zhou, Y., Rajapakse, R. K. N. D., & Graham, J. (1998). A coupled thermoporoelastic model with thermo-osmosis and thermal-filtration. *International Journal of Solids and Structures*, *35*(34-35), 4659-4683. https://doi.org/10.1016/S0020-7683(98)00089-4

List of symbols

$\sigma_z^{'}$ vertical effective stress

ε_z vertical strain

V initial specific volume ($V = 1 + e_0$)

κ slope of instant time line (unloading-reloading line) in $e - \ln \sigma_z^{'}$ space at T_0

λ slope of reference time line (normal compression line) in $e - \ln \sigma_z^{'}$ space at T_0

κ_T slope of elastic cooling-reheating line in $e - \ln T$ space

λ_T slope of virgin heating line in $e - \ln T$ space

ψ creep coefficient ($\psi = \dfrac{Vd\varepsilon_{creep}}{d\ln t}$)

$\sigma_{zp}^{'}$ pre-consolidation pressure (yielding stress)

ε_{zp} vertical strain under $\sigma_{zp}^{'}$ on the current equivalent time line

$\sigma_{zp0}^{'}$ reference pre-consolidation pressure on the reference time line at T_0

ε_{zp0} vertical strain under $\sigma_{zp0}^{'}$ on the reference time line at T_0

T_0 reference temperature

t_0 reference time

t_e equivalent time

$\dot{\varepsilon}_z^{vp}$ visco–plastic (creep) strain rate

Table 1. Basic physical properties of the tested soils

	Specific gravity, G_s	Liquid limit, LL	Plastic limit, PL	Plasticity index, PI
HKMD	2.61	49	31	18
Kaolin	2.52	59	32	27

Table 2. Loading and temperature scheme for the two specimens

	Vertical stress (kPa)	Temperature (℃)
Loading	5	20
	10	20
	20	20
	50	20
	100	20 → 40 → 20 → 40
	200	40 → 20
	400	20
Unloading	267	20 → 40
	133	40 → 20
	67	20 → 40 → 20
Loading	133	20
	267	20
	400	20 → 40 → 60 → 40 → 20 → 40 → 60
	800	60 → 40 → 20

Table 3. Parameters for TEVP model in the prediction

	e_0	$\frac{\psi}{V}$	t_0 (min)	$\frac{\kappa_T}{V}$	$\frac{\lambda_T}{V}$ 100kPa	200kPa	400kPa	800kPa
HKMD	1.42	0.0017	100	-0.0011	0.100	0.080	0.061	0.061
Kaolin	1.58	0.0006	100	0.0014	0.047	0.044	0.040	0.040

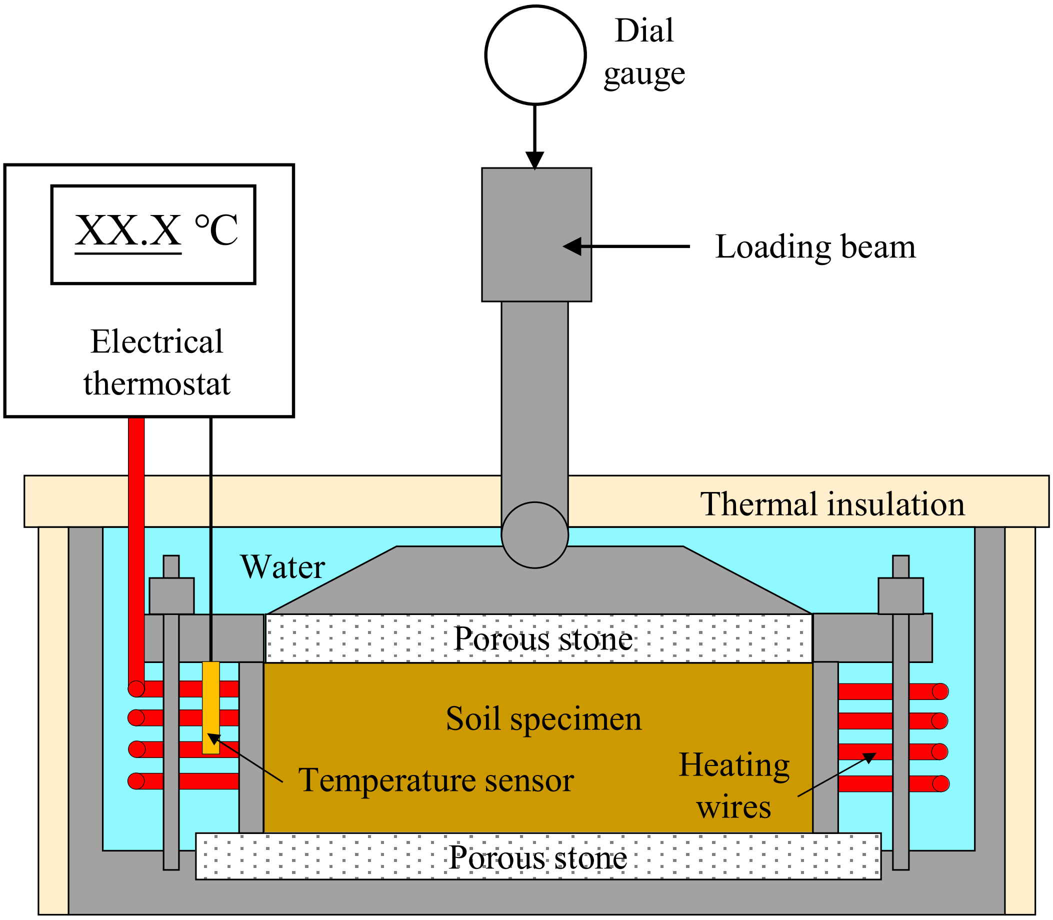
Dial
gauge
XX.X °C
Electrical
thermostat
Loading beam
Thermal insulation
Water
Porous stone
Soil specimen
Temperature sensor
Heating
wires
Porous stone

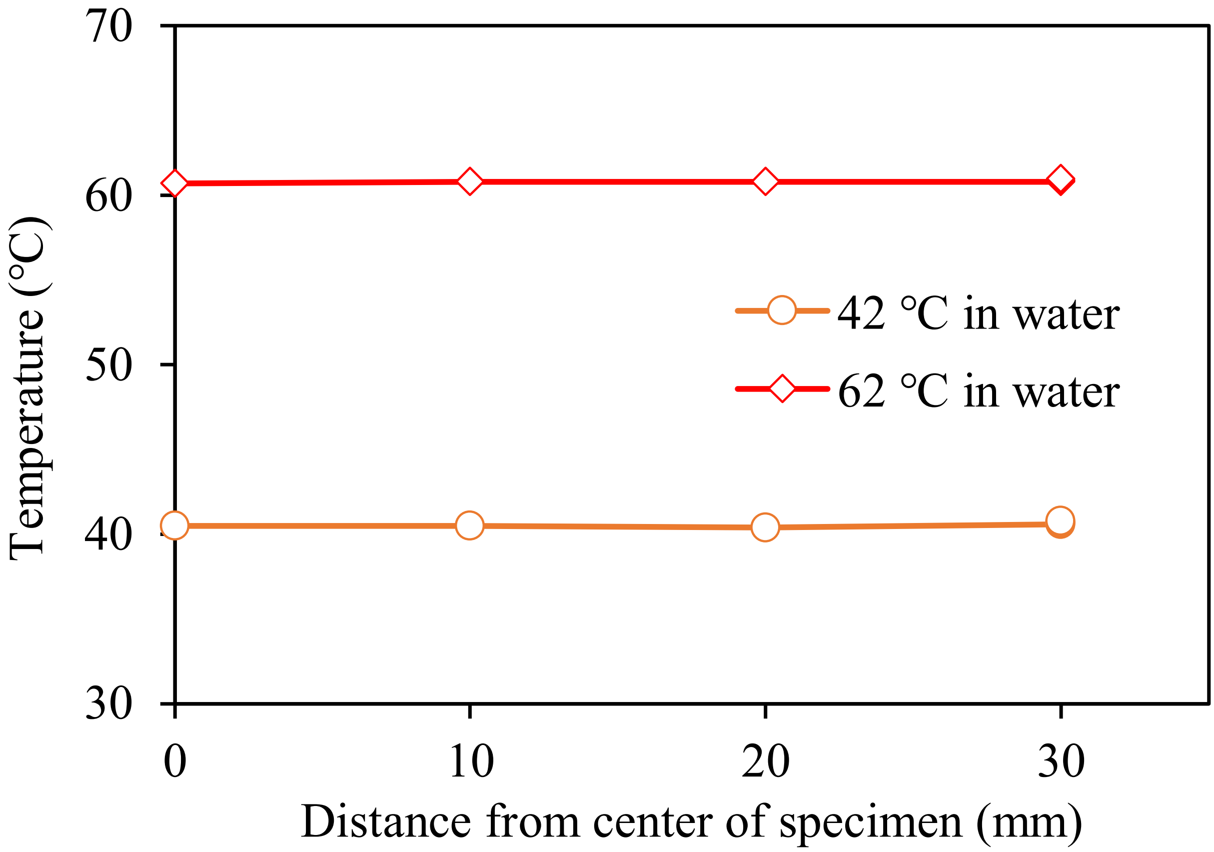
70
60
50
40
30
Temperature (°C)
0
10
20
30
Distance from center of specimen (mm)
42 °C in water
62 °C in water

Fig. 2b

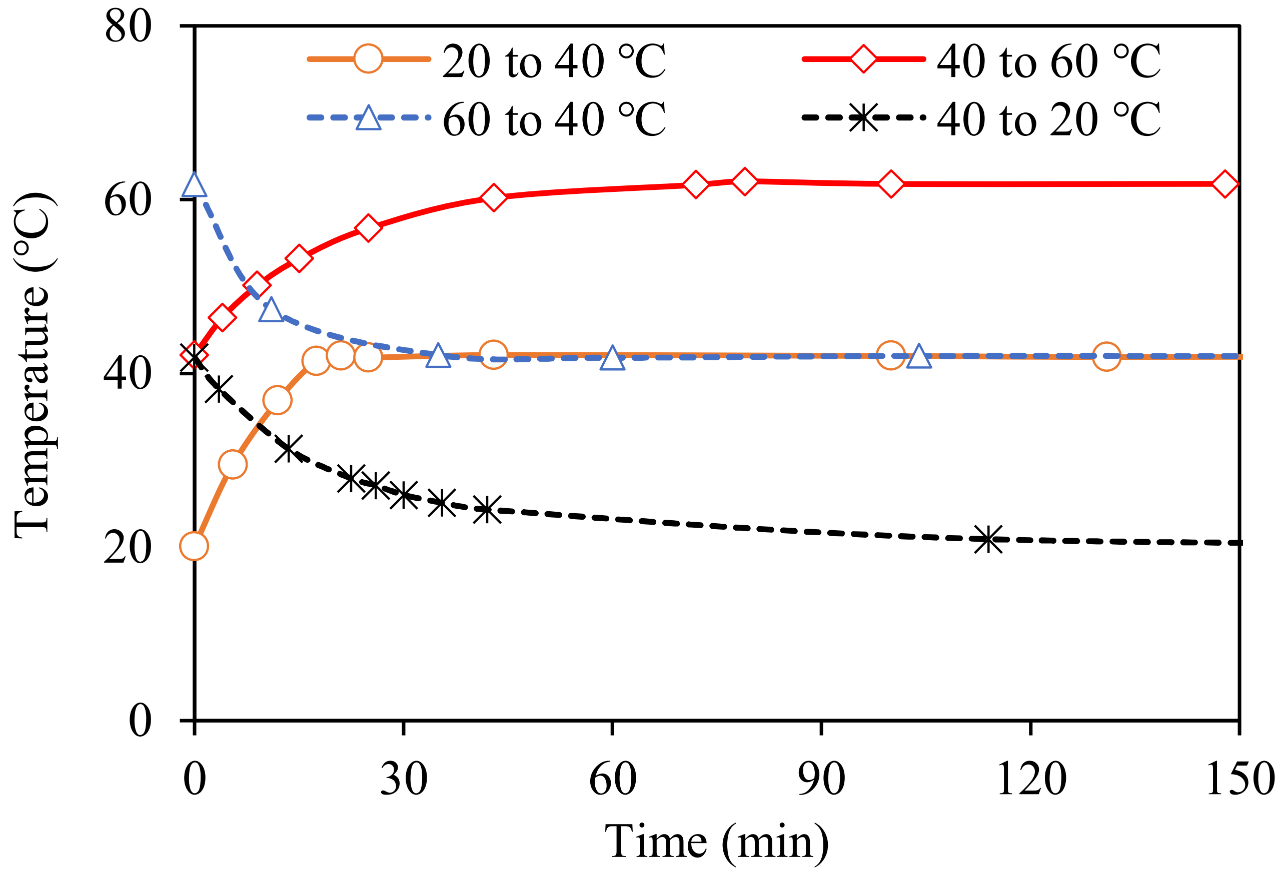
80
60
40
20
0
0
30
60
90
120
150
Time (min)
Temperature (°C)
20 to 40 °C
40 to 60 °C
60 to 40 °C
40 to 20 °C

Fig. 3

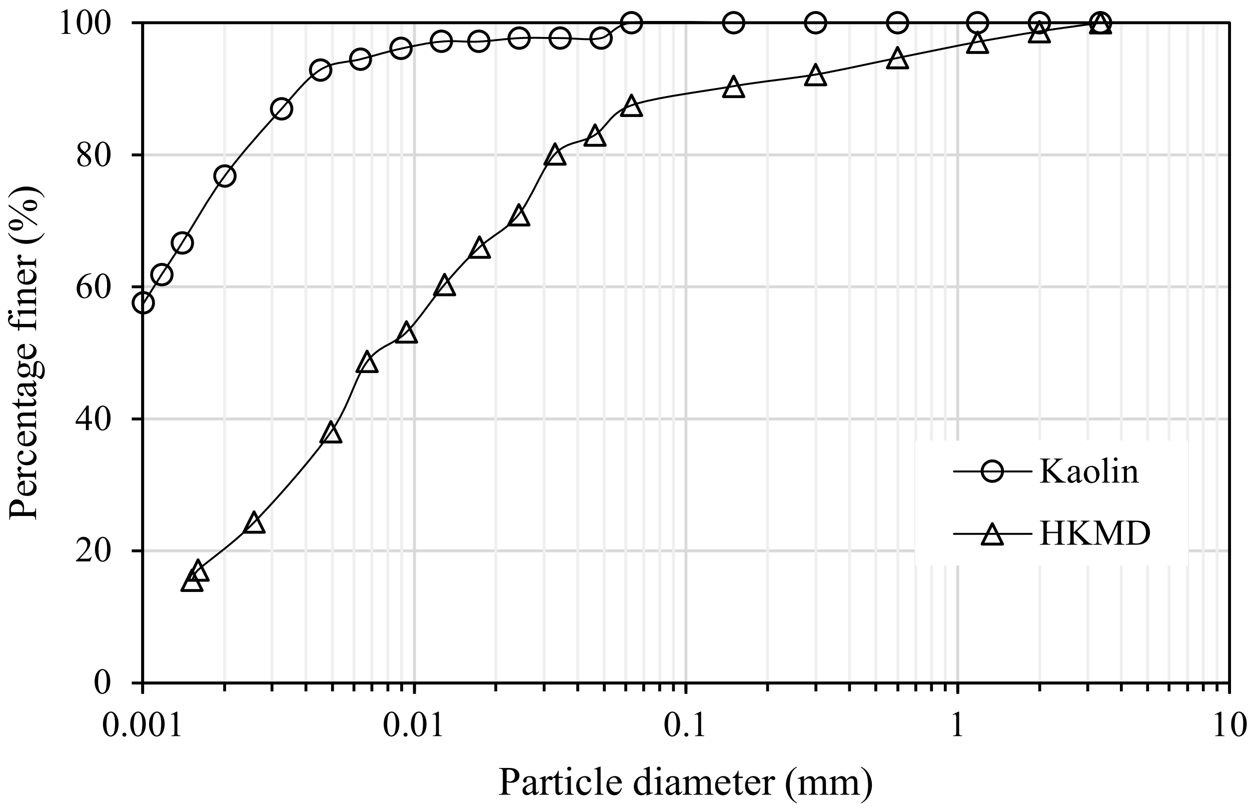

100
80
60
40
20
0
Percentage finer (%)
0.001
0.01
0.1
1
10
Particle diameter (mm)
Kaolin
HKMD

Fig. 4

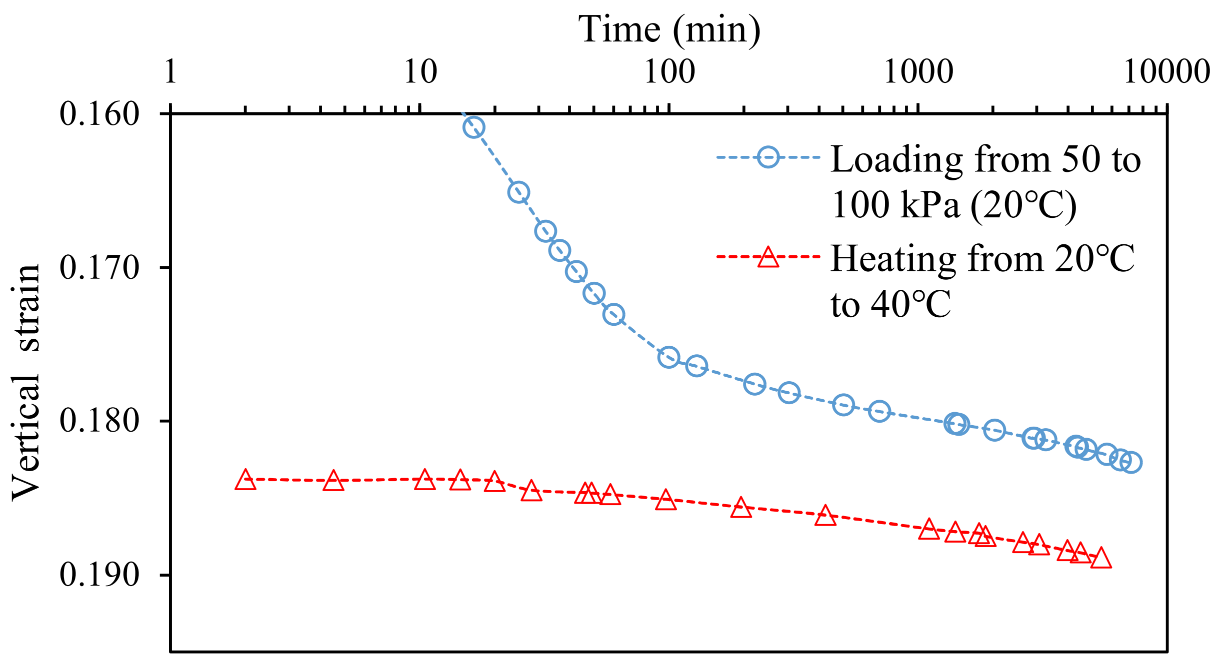

Time (min)
1
10
100
1000
10000
0.160
0.170
0.180
0.190
Vertical strain
Loading from 50 to 100 kPa (20°C)
Heating from 20°C to 40°C

Fig. 5a

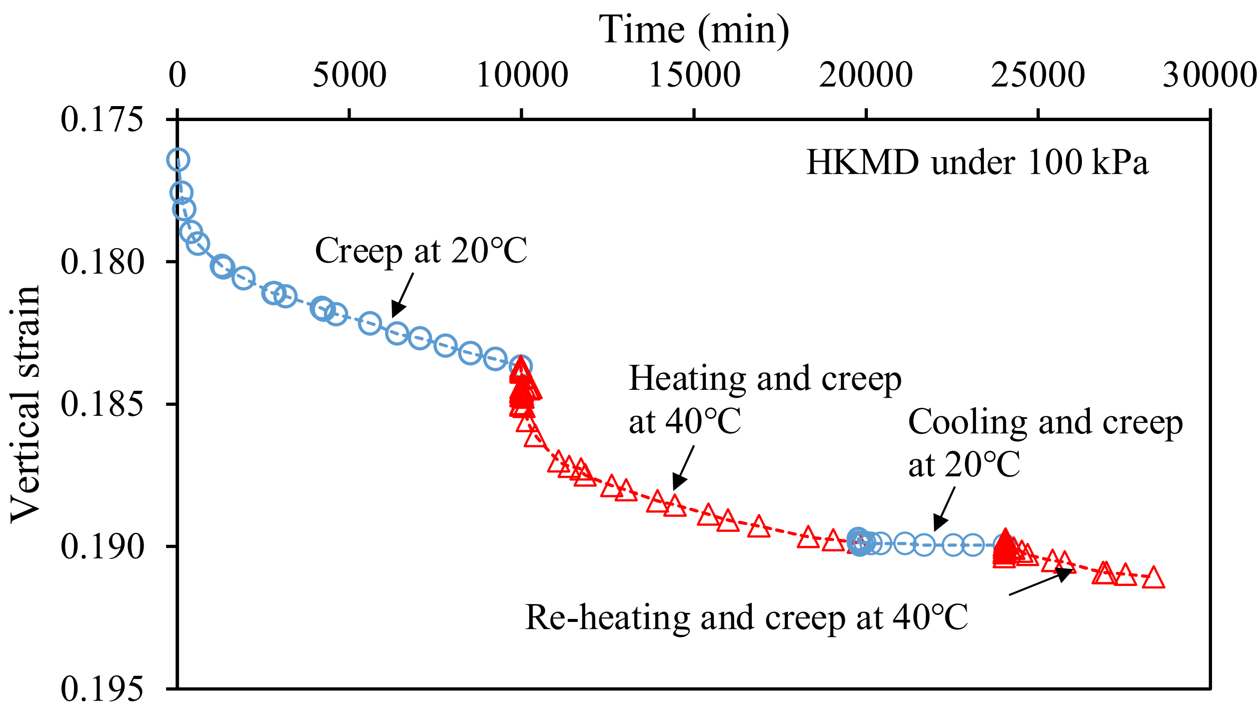

Time (min)
0
5000
10000
15000
20000
25000
30000
0.175
0.180
0.185
0.190
0.195
Vertical strain
HKMD under 100 kPa
Creep at 20°C
Heating and creep
at 40°C
Cooling and creep
at 20°C
Re-heating and creep at 40°C

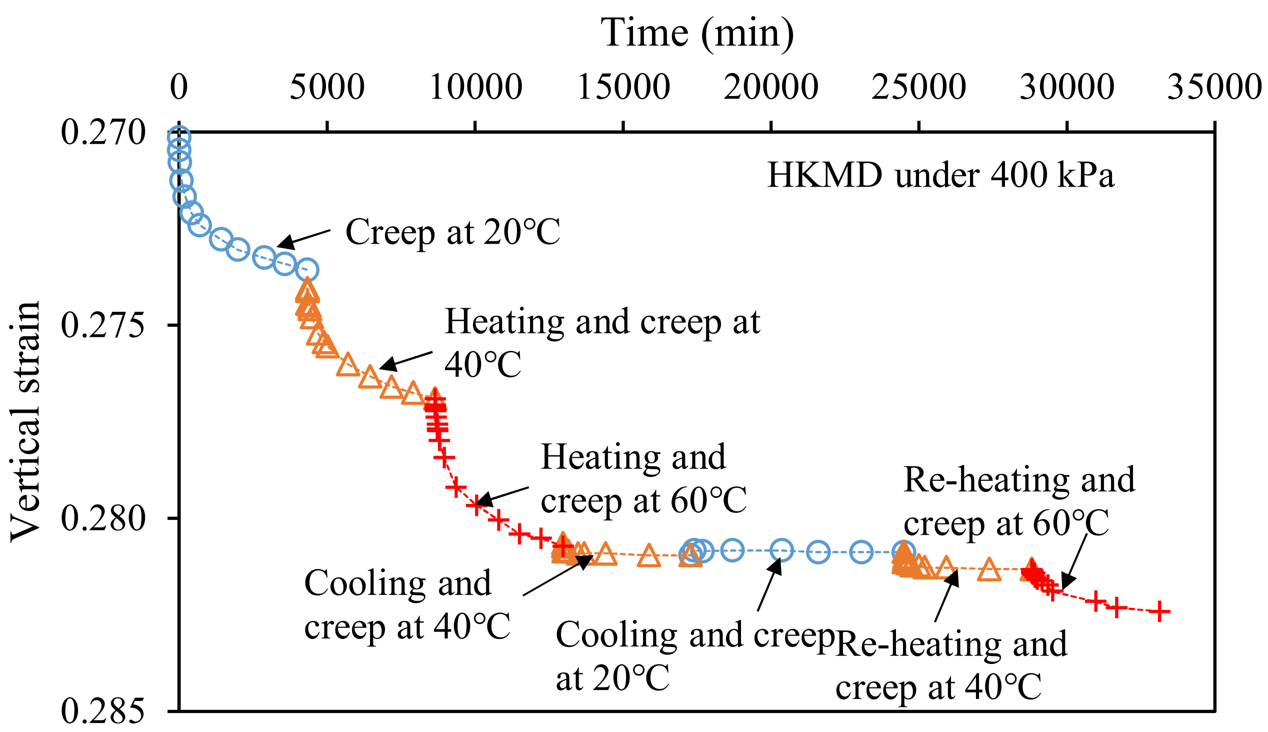
Time (min)
0
5000
10000
15000
20000
25000
30000
35000
0.270
0.275
0.280
0.285
Vertical strain
HKMD under 400 kPa
Creep at 20°C
Heating and creep at 40°C
Heating and creep at 60°C
Cooling and creep at 40°C
Cooling and creep at 20°C
Re-heating and creep at 40°C
Re-heating and creep at 60°C

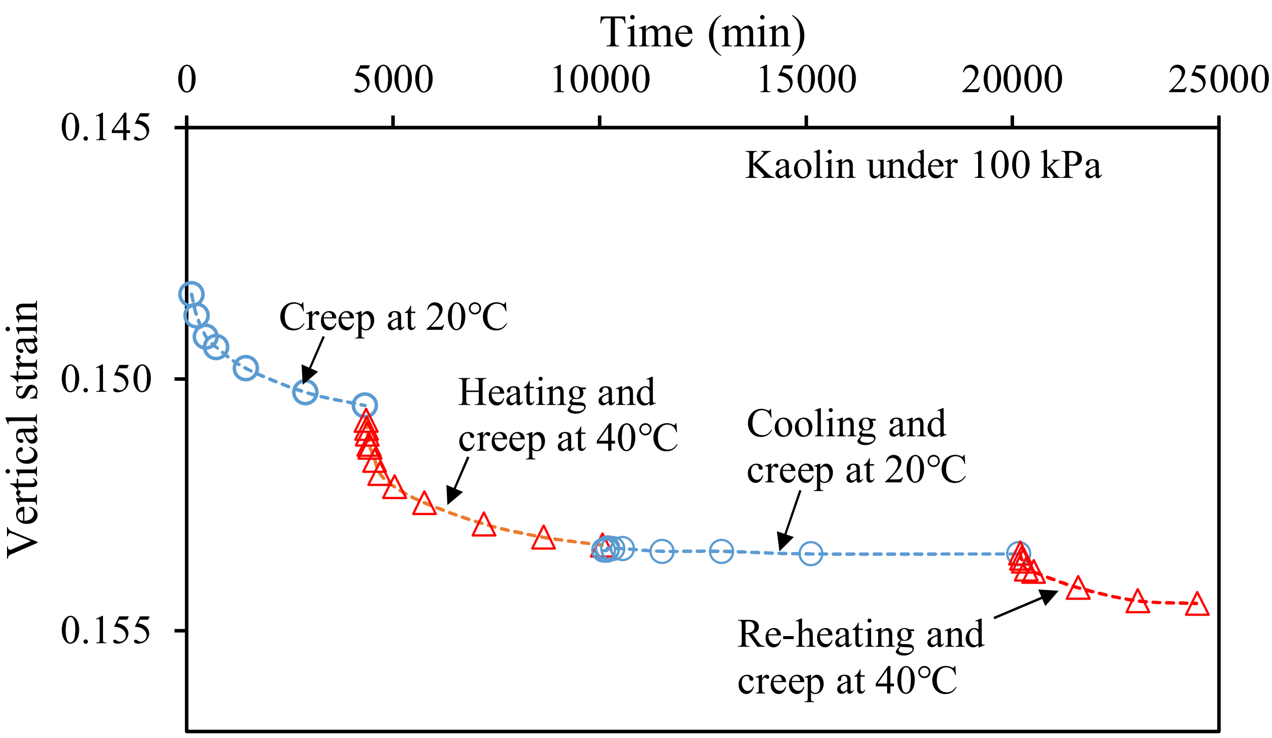
Time (min)
0
5000
10000
15000
20000
25000
0.145
0.150
0.155
Vertical strain
Kaolin under 100 kPa
Creep at 20°C
Heating and
creep at 40°C
Cooling and
creep at 20°C
Re-heating and
creep at 40°C

Fig. 5d

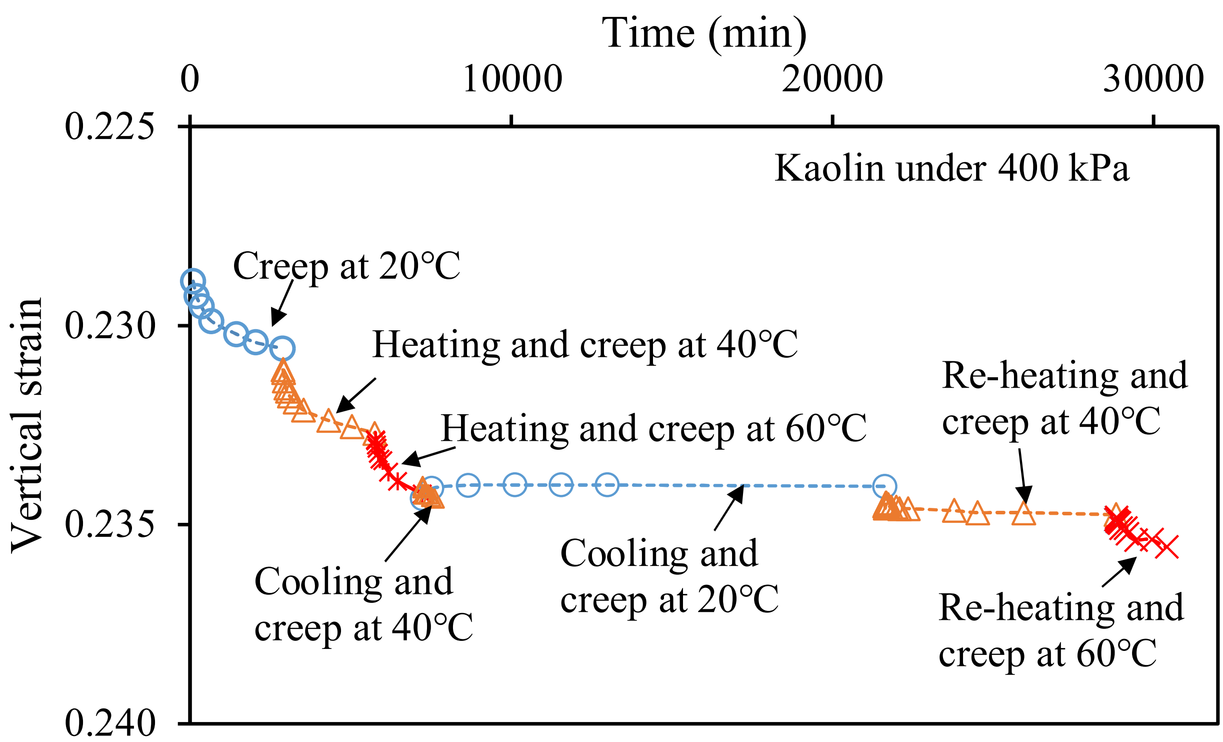

Time (min)
0
10000
20000
30000
0.225
0.230
0.235
0.240
Vertical strain
Kaolin under 400 kPa
Creep at 20°C
Heating and creep at 40°C
Heating and creep at 60°C
Re-heating and creep at 40°C
Cooling and creep at 40°C
Cooling and creep at 20°C
Re-heating and creep at 60°C

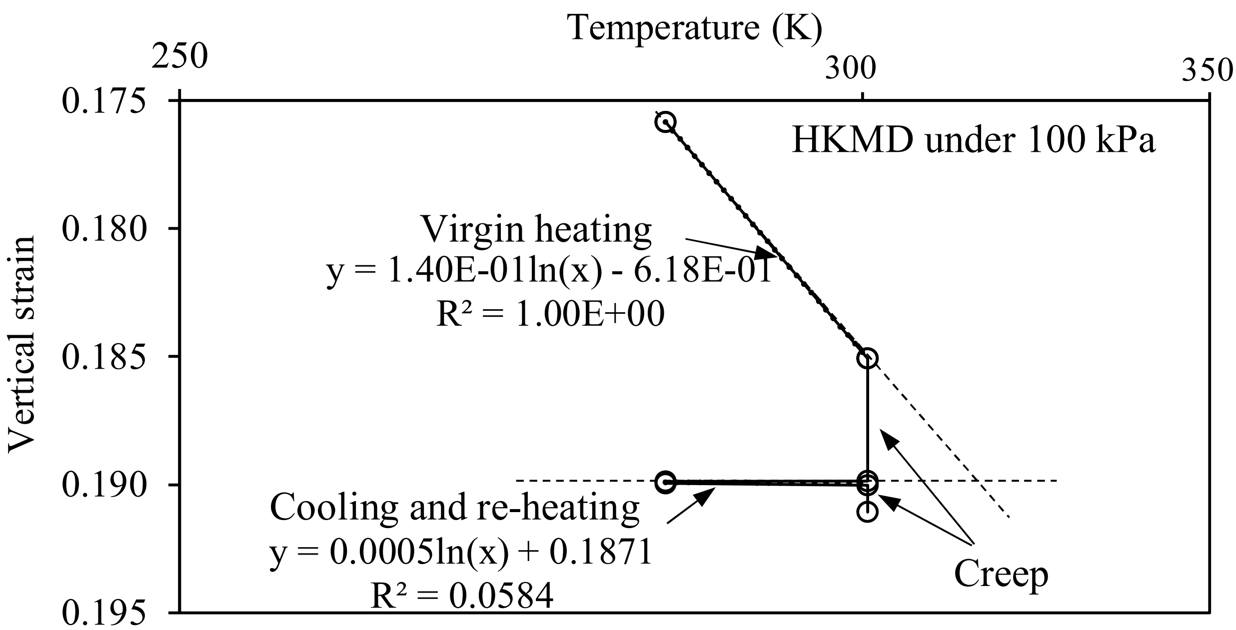
Temperature (K)
250
300
350
0.175
0.180
0.185
0.190
0.195
Vertical strain
HKMD under 100 kPa
Virgin heating
y = 1.40E-01ln(x) - 6.18E-01
R² = 1.00E+00
Cooling and re-heating
y = 0.0005ln(x) + 0.1871
R² = 0.0584
Creep

Fig. 6b

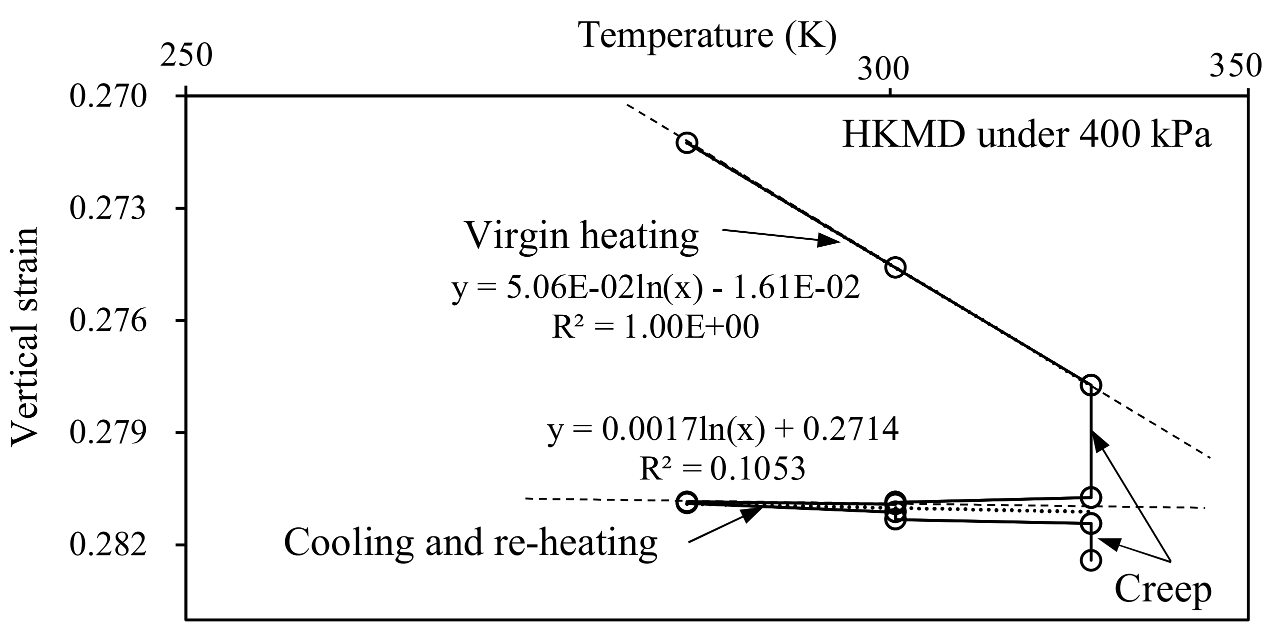
Temperature (K)
250
300
350
0.270
0.273
0.276
0.279
0.282
Vertical strain
HKMD under 400 kPa
Virgin heating
y = 5.06E-02ln(x) - 1.61E-02
R² = 1.00E+00
y = 0.0017ln(x) + 0.2714
R² = 0.1053
Cooling and re-heating
Creep

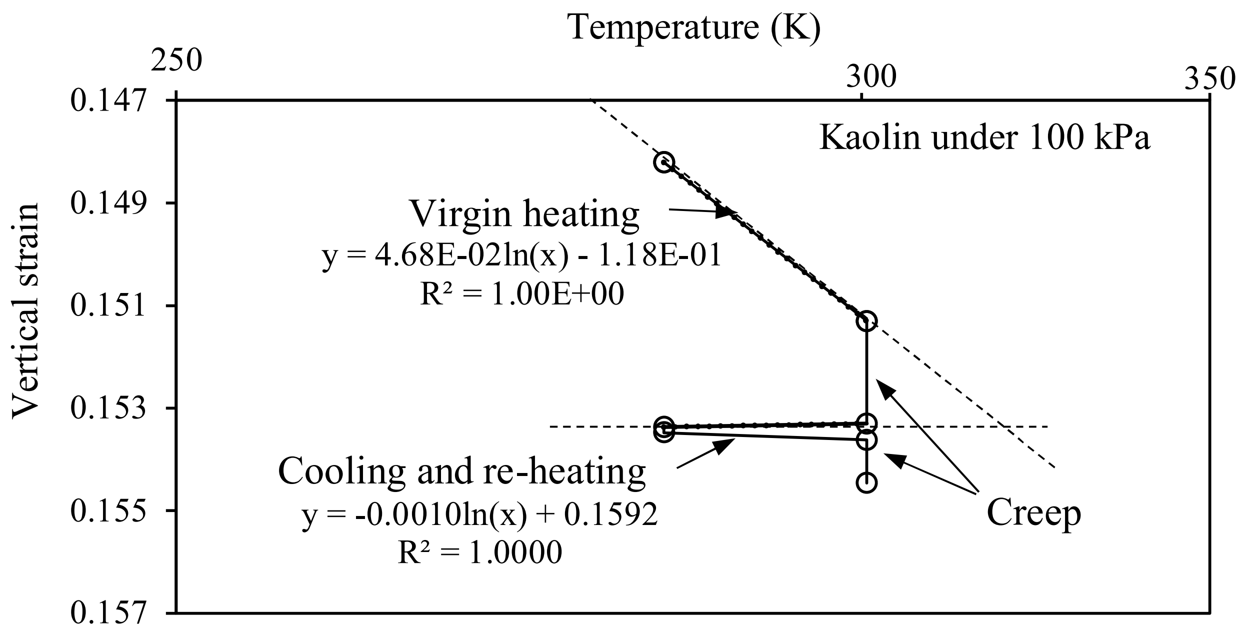
Temperature (K)
250
300
350
0.147
0.149
0.151
0.153
0.155
0.157
Vertical strain
Kaolin under 100 kPa
Virgin heating
y = 4.68E-02ln(x) - 1.18E-01
R² = 1.00E+00
Cooling and re-heating
y = -0.0010ln(x) + 0.1592
R² = 1.0000
Creep

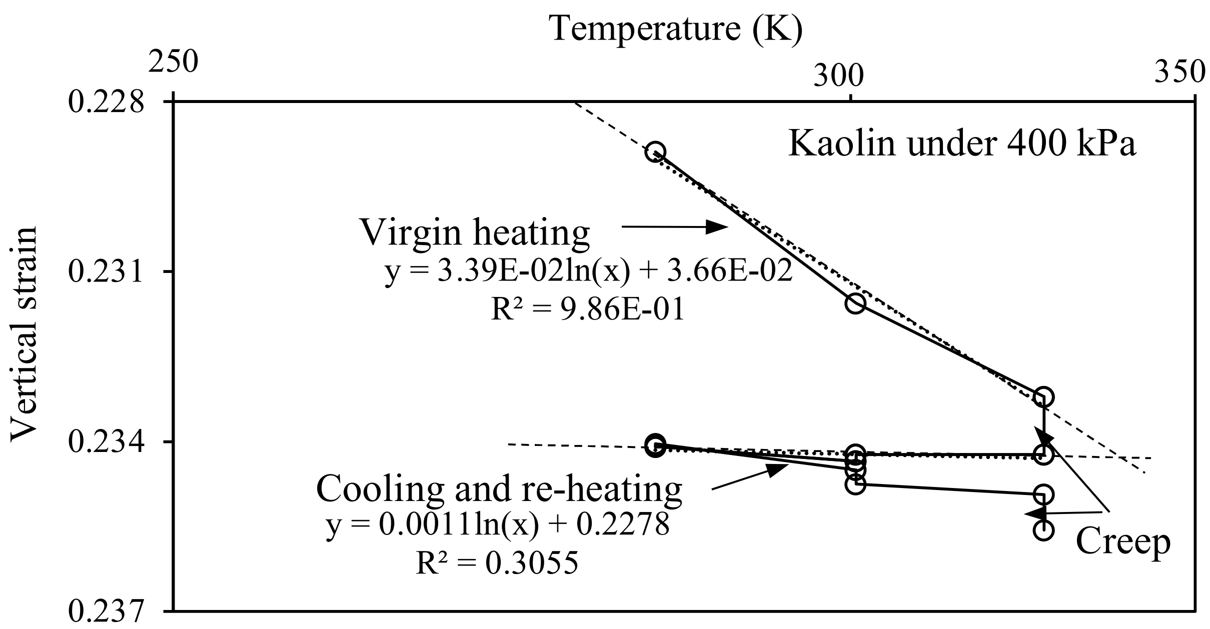
Temperature (K)
250
300
350
0.228
0.231
0.234
0.237
Vertical strain
Kaolin under 400 kPa
Virgin heating
y = 3.39E-02ln(x) + 3.66E-02
R² = 9.86E-01
Cooling and re-heating
y = 0.0011ln(x) + 0.2278
R² = 0.3055
Creep

Fig. 7

Click here to access/download;Figure;Fig 7.pdf

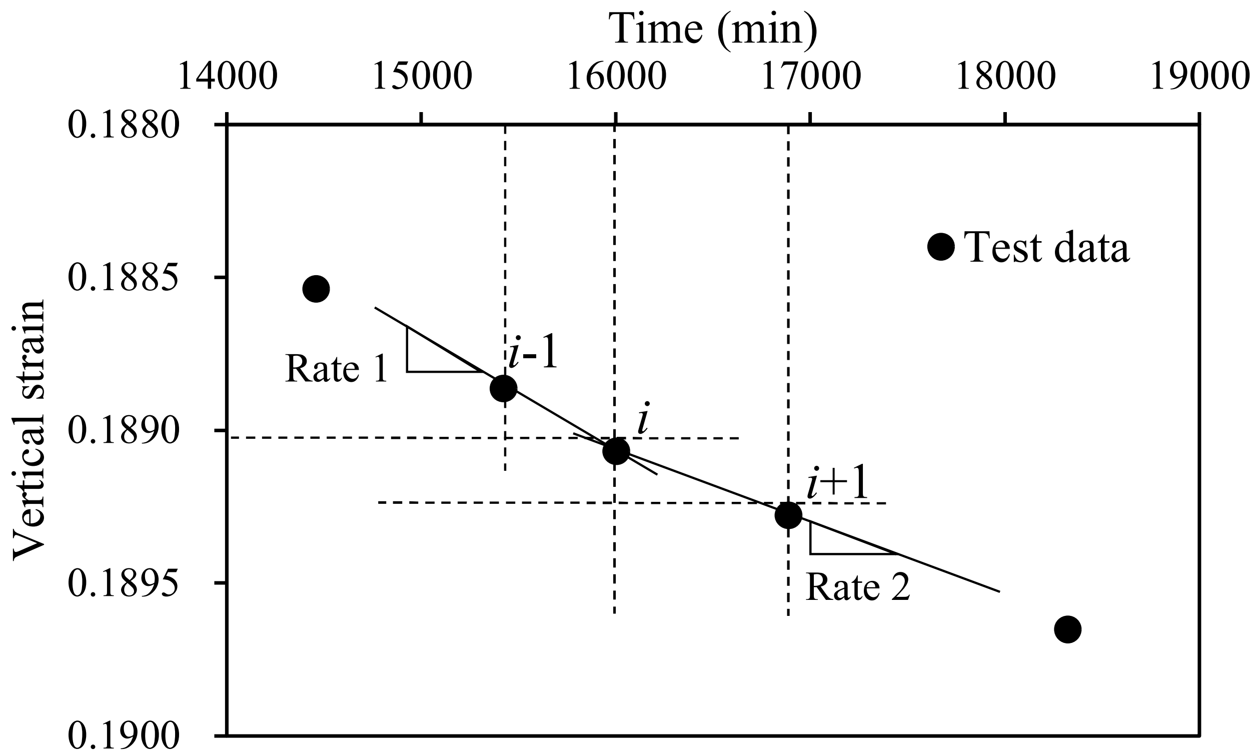

Fig. 8a

Click here to access/download;Figure;Fig 8a.pdf

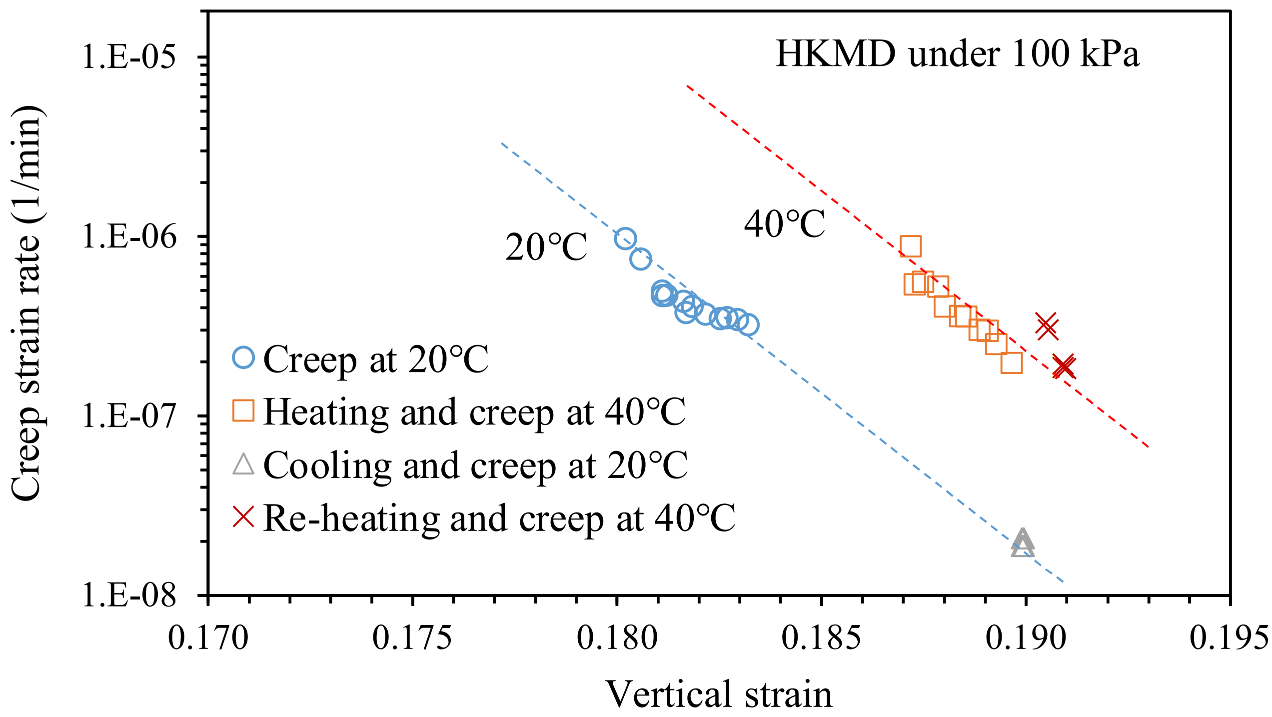

Fig. 8b

Click here to access/download;Figure;Fig 8b.pdf

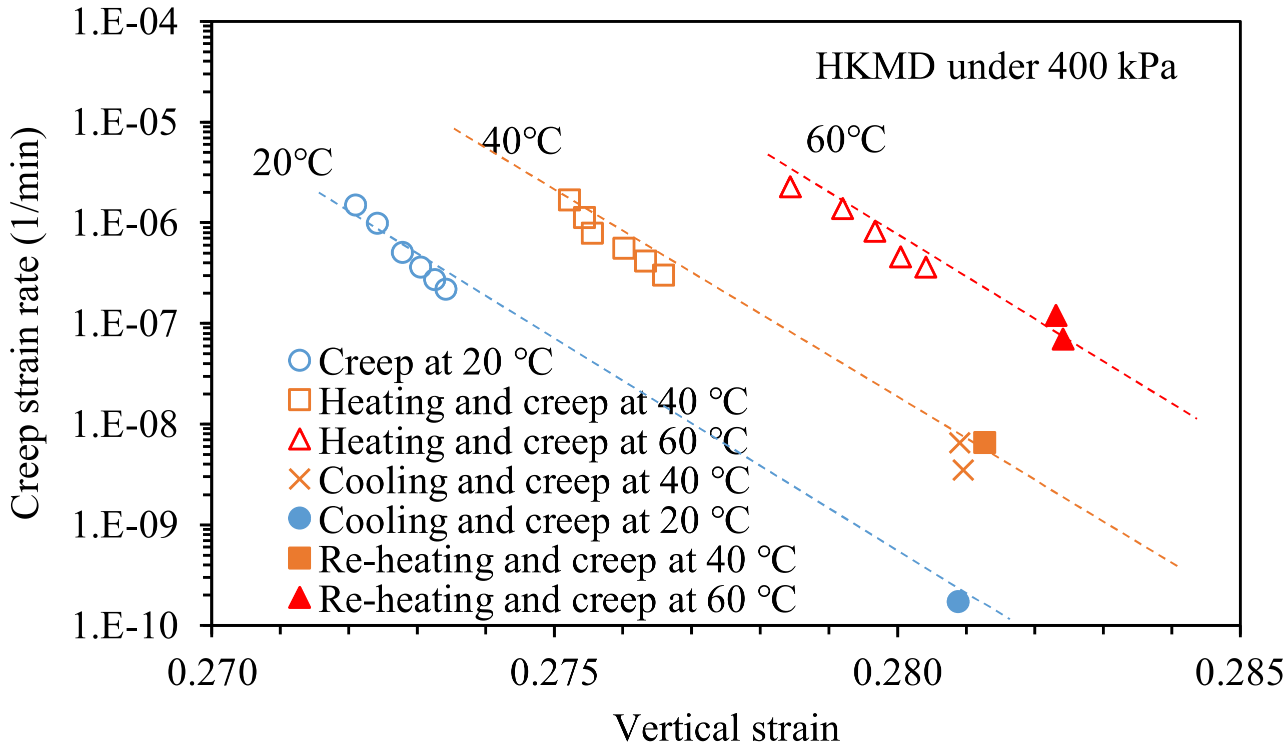

Fig. 8c

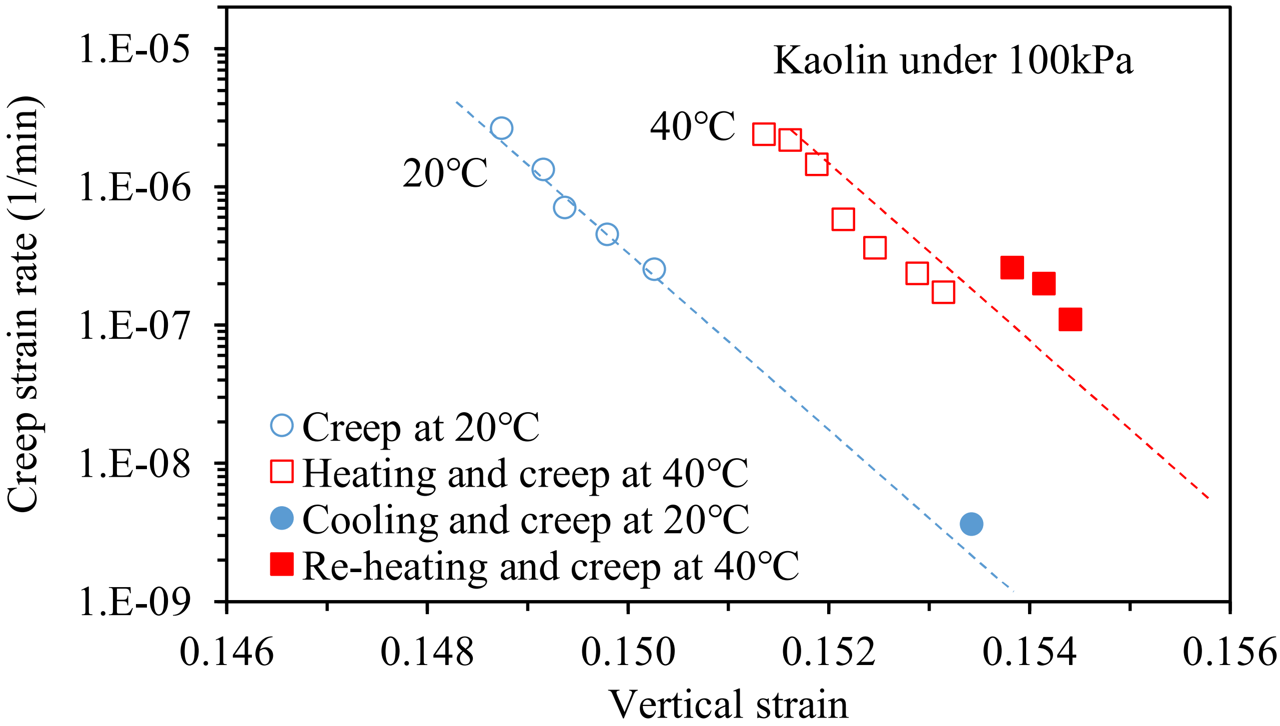
Kaolin under 100kPa
40°C
20°C
Creep strain rate (1/min)
1.E-05
1.E-06
1.E-07
1.E-08
1.E-09
Creep at 20°C
Heating and creep at 40°C
Cooling and creep at 20°C
Re-heating and creep at 40°C
0.146
0.148
0.150
0.152
0.154
0.156
Vertical strain

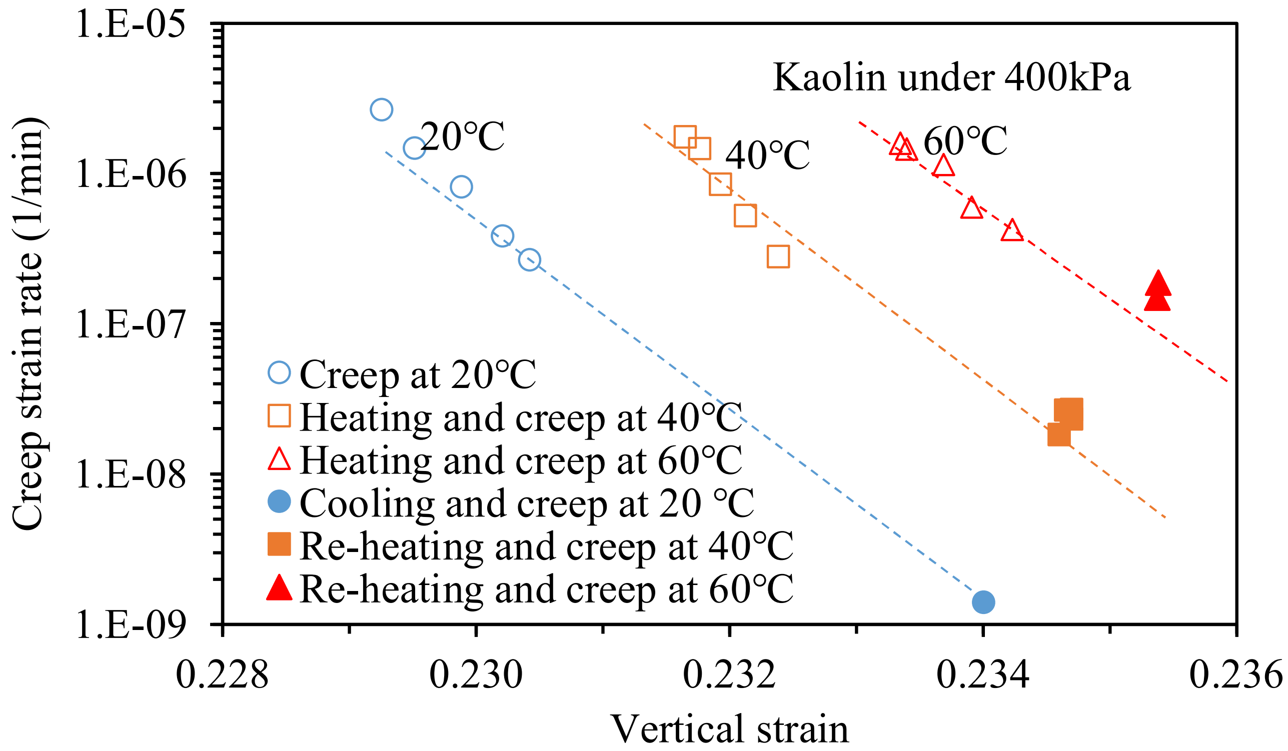
1.E-05
1.E-06
1.E-07
1.E-08
1.E-09
Creep strain rate (1/min)
Kaolin under 400kPa
20°C
40°C
60°C
Creep at 20°C
Heating and creep at 40°C
Heating and creep at 60°C
Cooling and creep at 20 °C
Re-heating and creep at 40°C
Re-heating and creep at 60°C
0.228
0.230
0.232
0.234
0.236
Vertical strain

Fig. 9a

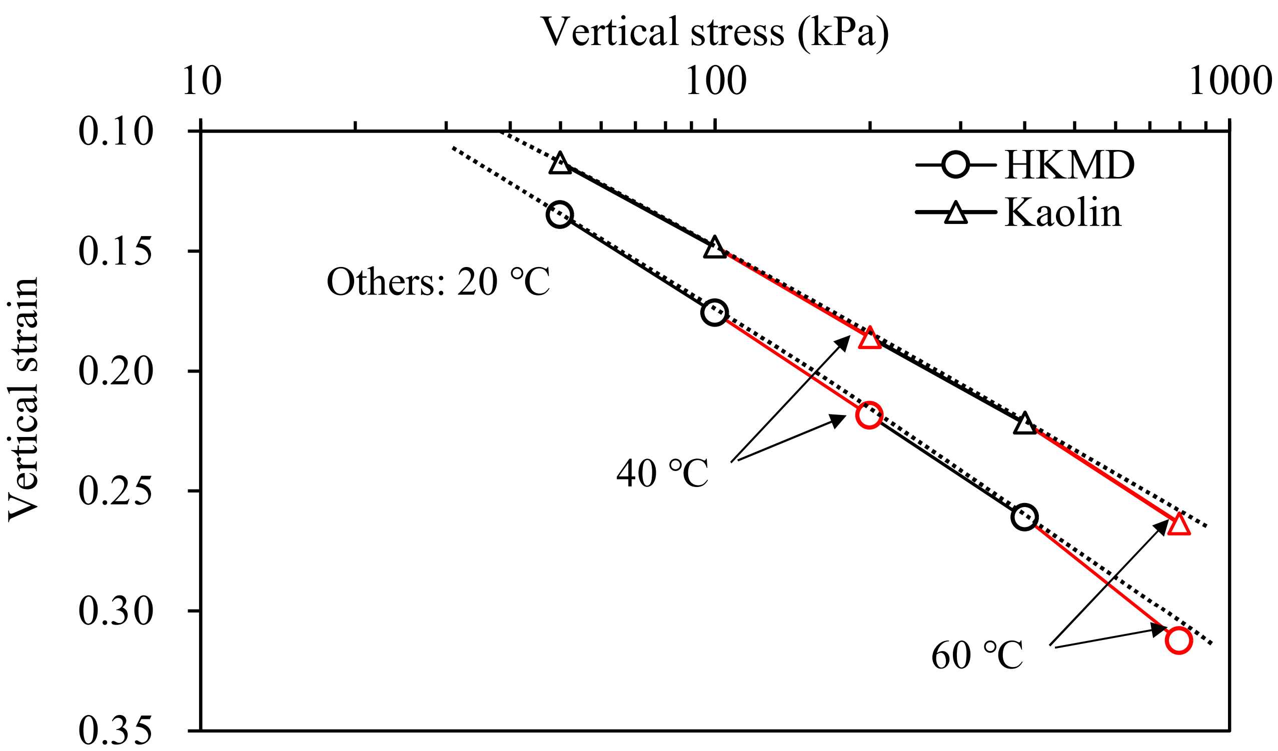

Vertical stress (kPa)
10
100
1000
0.10
0.15
0.20
0.25
0.30
0.35
Vertical strain
HKMD
Kaolin
Others: 20 °C
40 °C
60 °C

Fig. 9b

Click here to access/download;Figure;Fig 9b.pdf

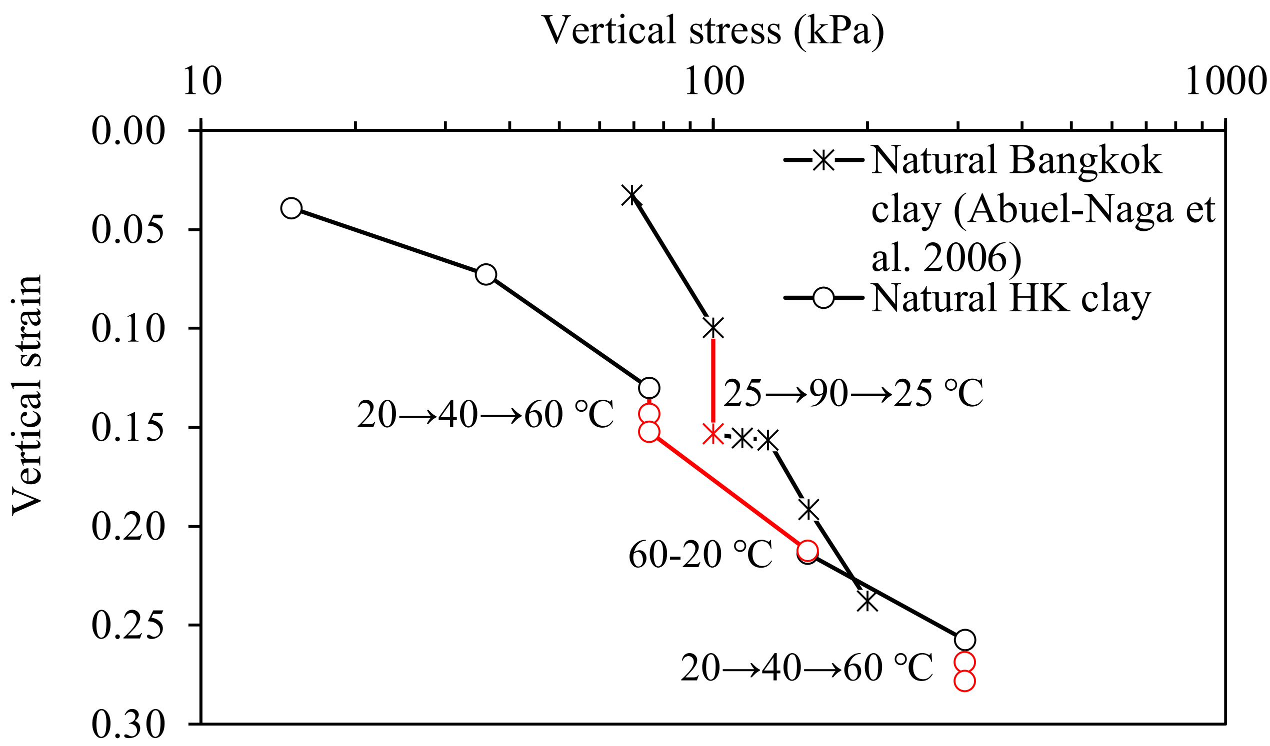

Fig. 10

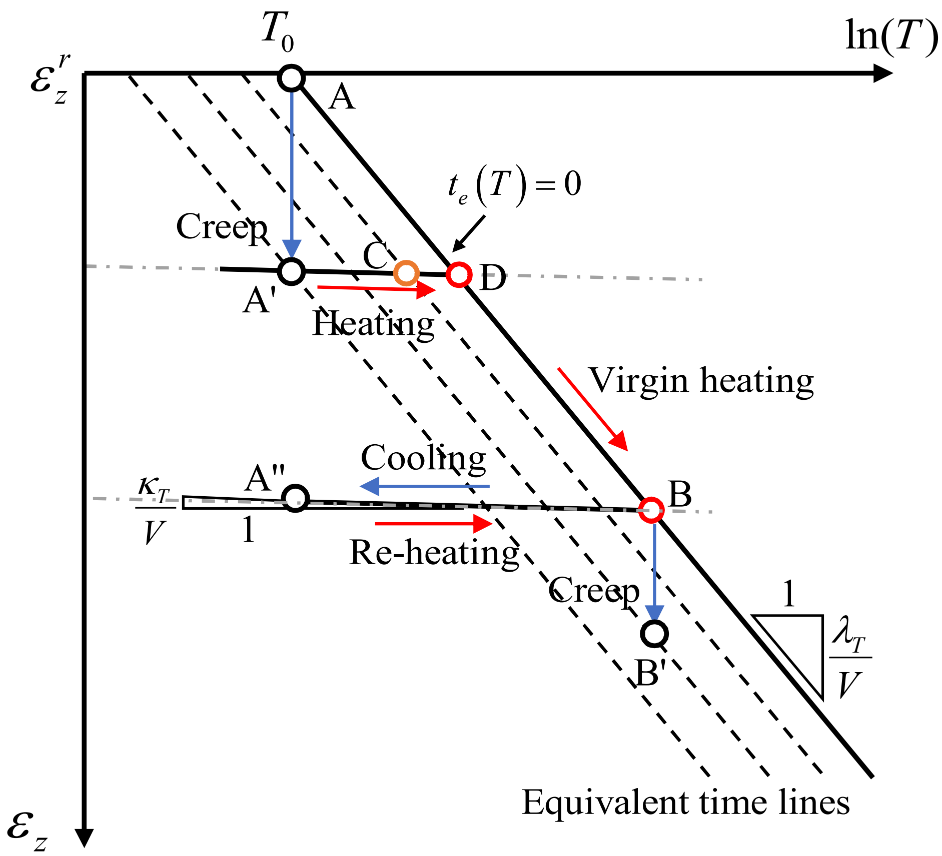

T_0
$\ln(T)$
ε_z^r
A
$t_e(T)=0$
Creep
C
A'
D
Heating
Virgin heating
$\frac{\kappa_T}{V}$
A''
Cooling
B
1
Re-heating
Creep
B'
1
$\frac{\lambda_T}{V}$
Equivalent time lines
ε_z

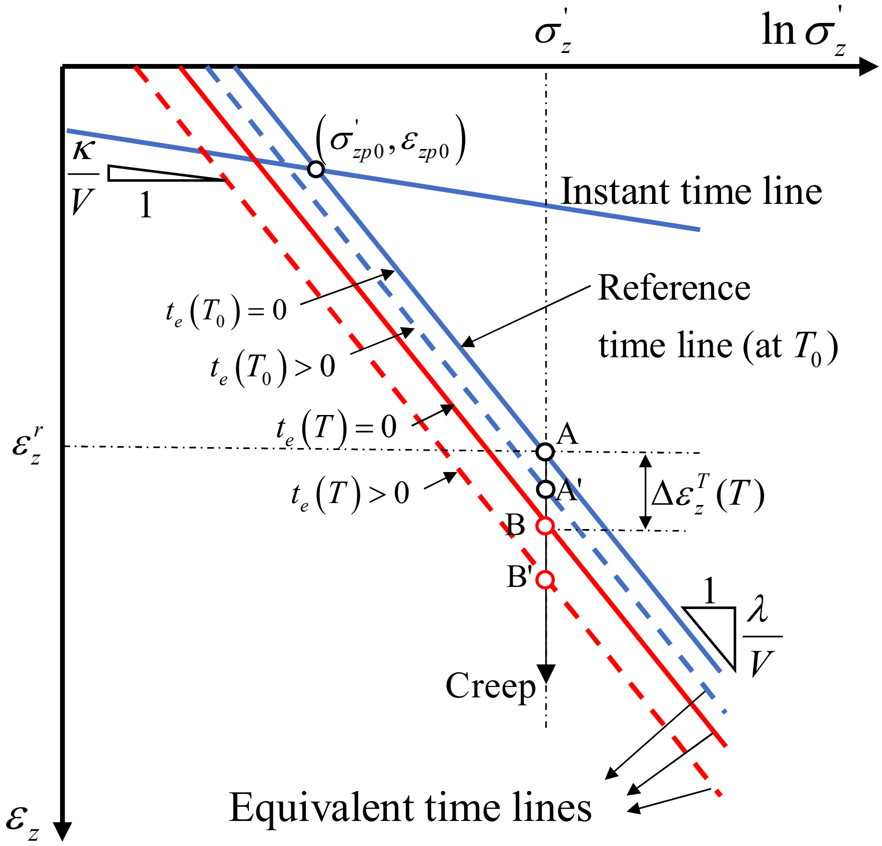

σ_z'
$\ln \sigma_z'$
$(\sigma_{zp0}', \varepsilon_{zp0})$
$\frac{\kappa}{V}$
1
Instant time line
Reference
time line (at T_0)
$t_e(T_0) = 0$
$t_e(T_0) > 0$
$t_e(T) = 0$
$t_e(T) > 0$
ε_z^r
A
A'
B
B'
$\Delta\varepsilon_z^T(T)$
1
$\frac{\lambda}{V}$
Creep
Equivalent time lines
ε_z

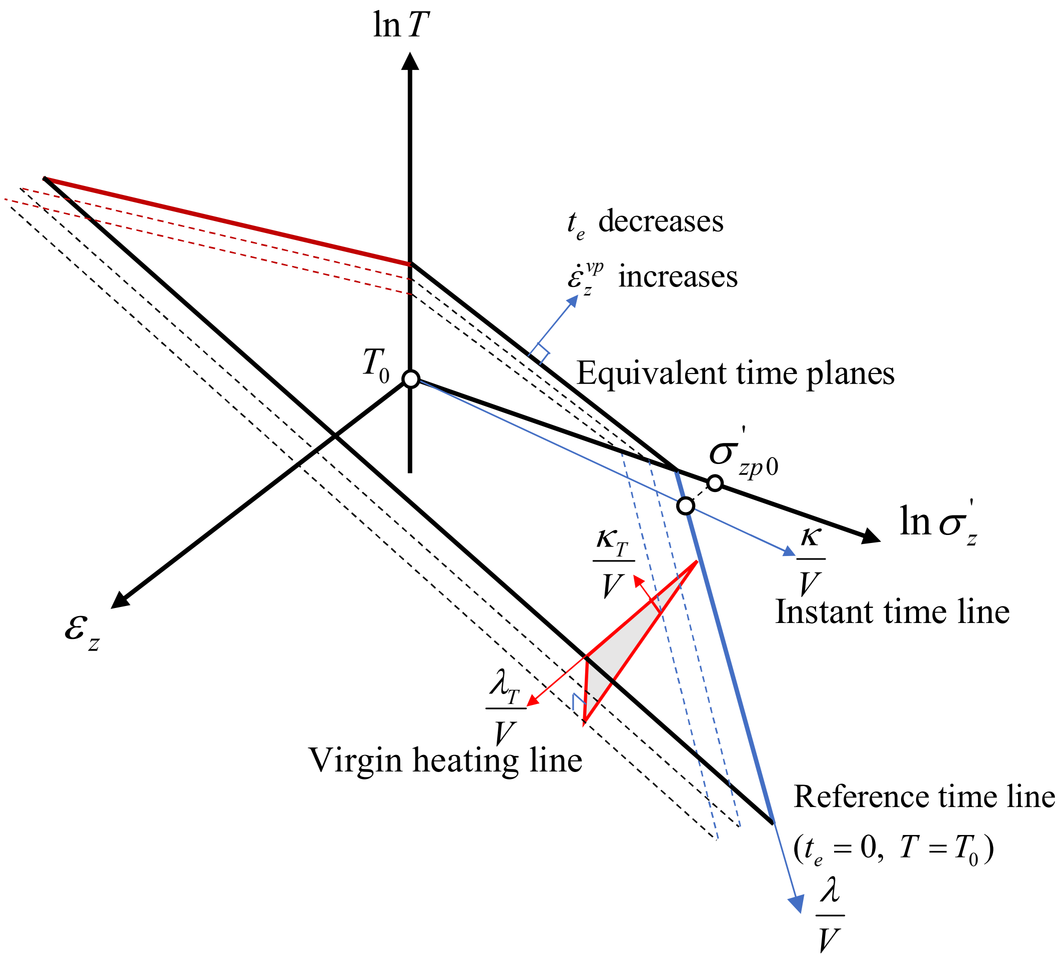
ln T
t_e decreases
ε̇_z^vp increases
T_0
Equivalent time planes
σ'_zp0
ln σ'_z
κ_T / V
κ / V
Instant time line
ε_z
λ_T / V
Virgin heating line
Reference time line
(t_e = 0, T = T_0)
λ / V

Fig. 13a

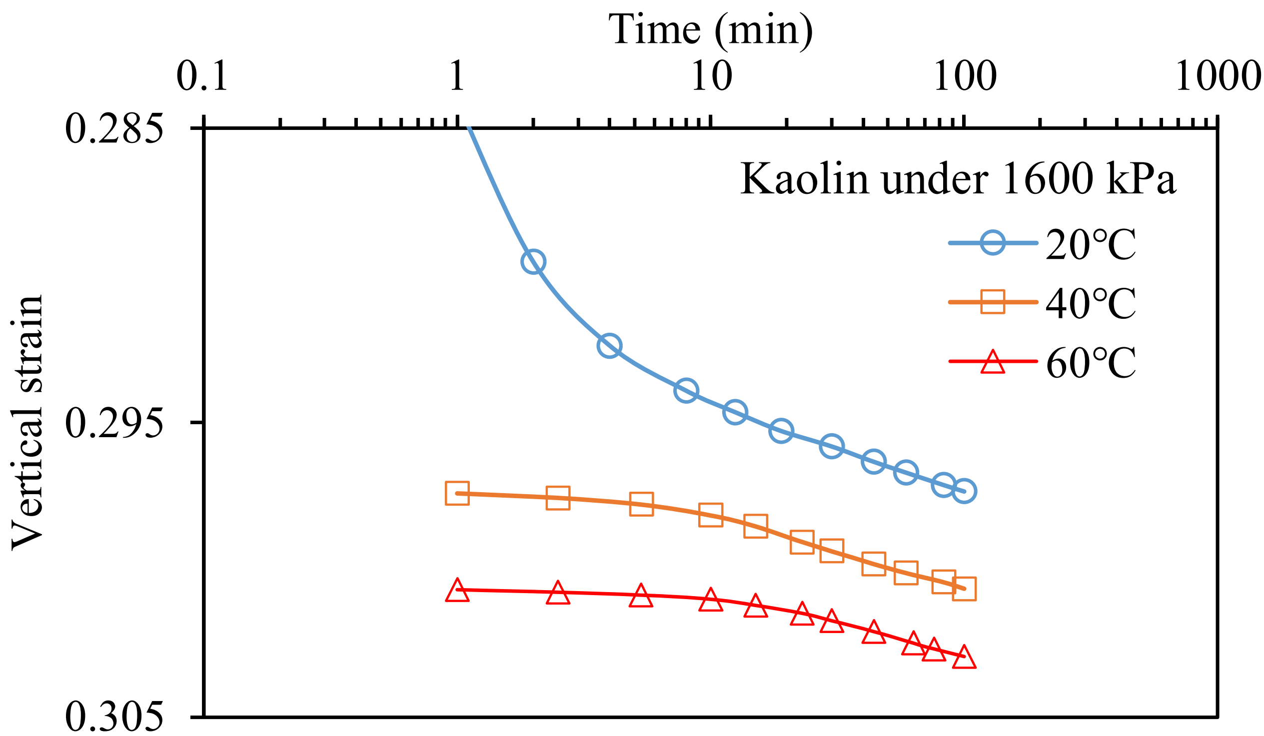
Time (min)
0.1
1
10
100
1000
0.285
0.295
0.305
Vertical strain
Kaolin under 1600 kPa
20°C
40°C
60°C

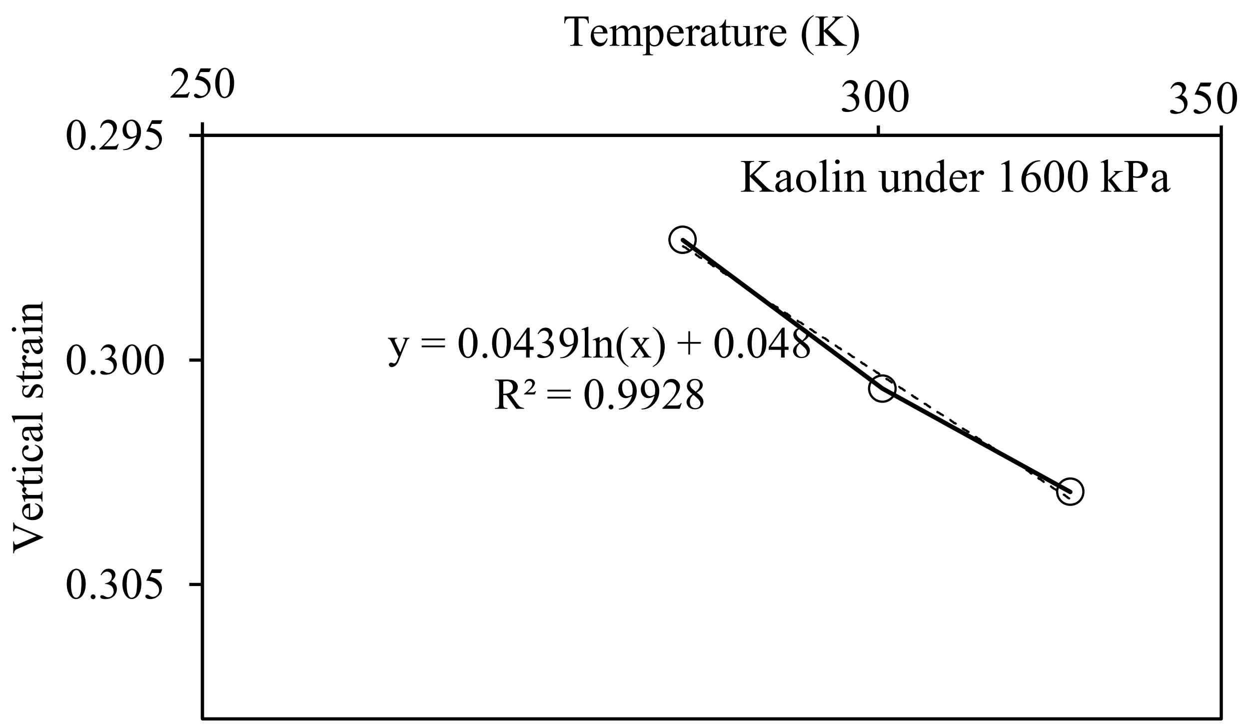
Temperature (K)
250
300
350
0.295
0.300
0.305
Vertical strain
Kaolin under 1600 kPa
y = 0.0439ln(x) + 0.048
R² = 0.9928

Fig. 14

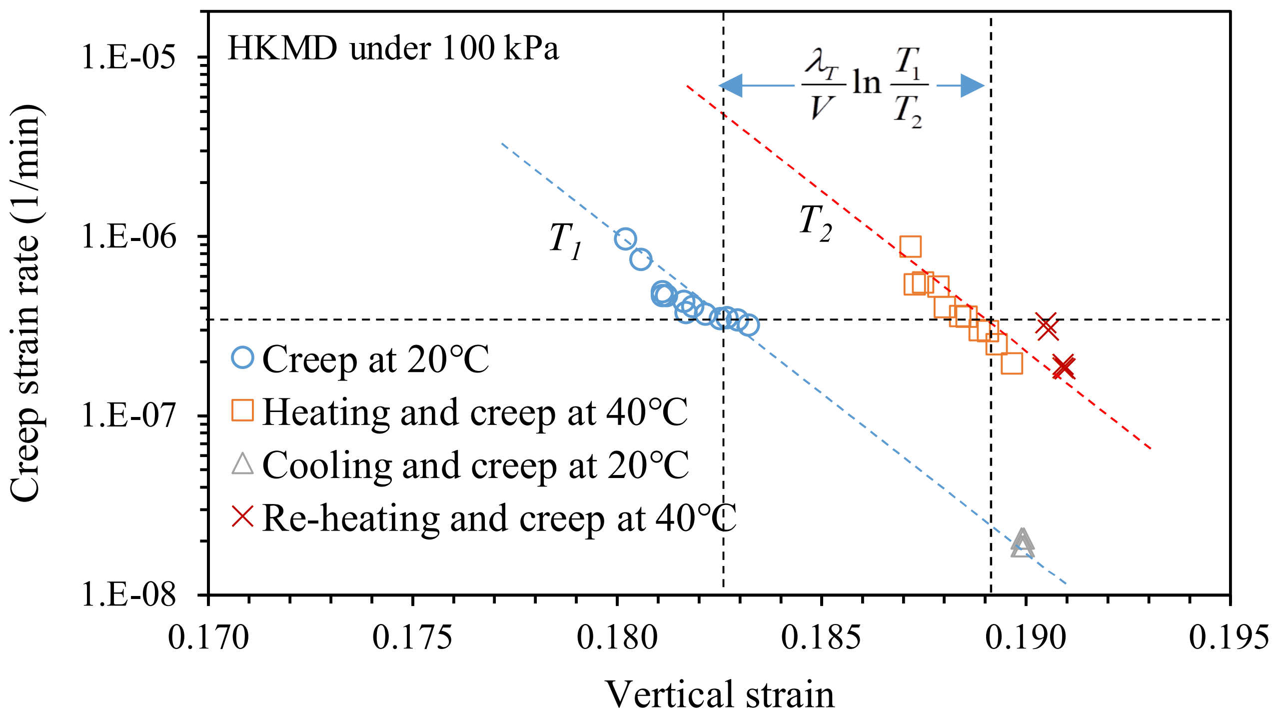

HKMD under 100 kPa
$\frac{\lambda_T}{V}\ln\frac{T_1}{T_2}$
T_1
T_2
Creep at 20°C
Heating and creep at 40°C
Cooling and creep at 20°C
Re-heating and creep at 40°C
Creep strain rate (1/min)
1.E-05
1.E-06
1.E-07
1.E-08
0.170
0.175
0.180
0.185
0.190
0.195
Vertical strain

Fig. 15

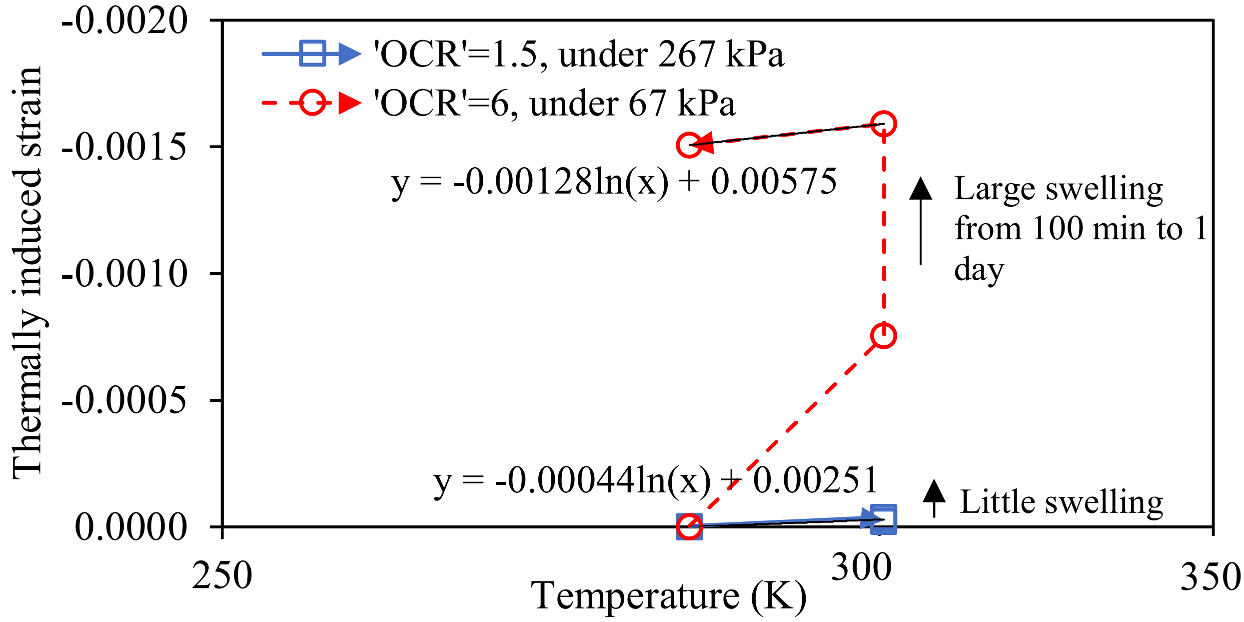
-0.0020
-0.0015
-0.0010
-0.0005
0.0000
Thermally induced strain
250
300
350
Temperature (K)
'OCR'=1.5, under 267 kPa
'OCR'=6, under 67 kPa
y = -0.00128ln(x) + 0.00575
y = -0.00044ln(x) + 0.00251
Large swelling from 100 min to 1 day
Little swelling

Fig. 16a

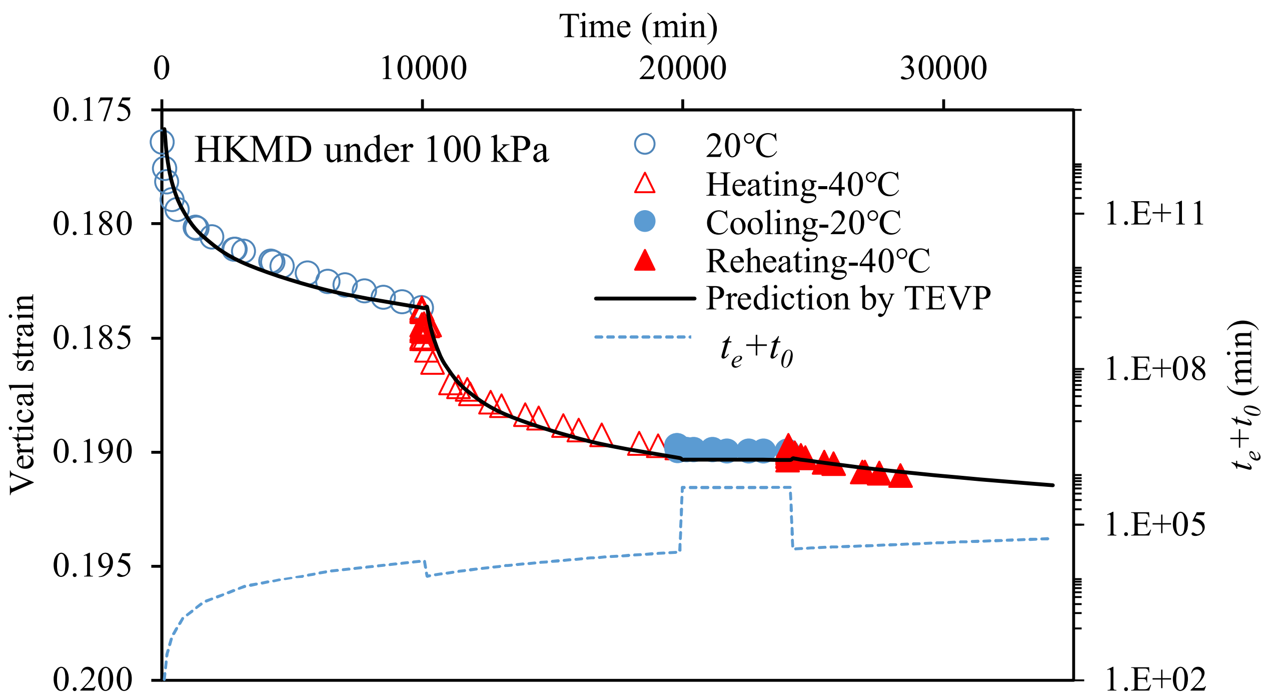
Time (min)
0
10000
20000
30000
0.175
0.180
0.185
0.190
0.195
0.200
Vertical strain
HKMD under 100 kPa
20°C
Heating-40°C
Cooling-20°C
Reheating-40°C
Prediction by TEVP
t_e+t_0
1.E+11
1.E+08
1.E+05
1.E+02
t_e+t_0 (min)

Fig. 16b

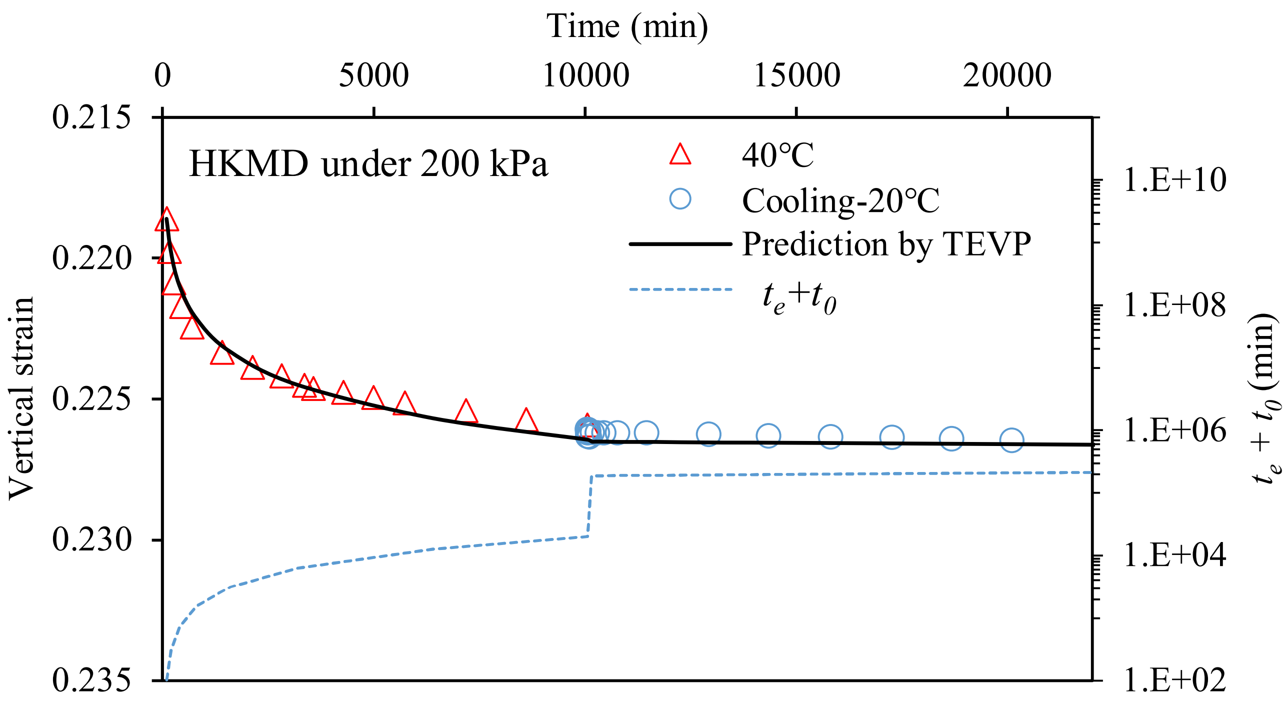

Time (min)
0
5000
10000
15000
20000
0.215
0.220
0.225
0.230
0.235
Vertical strain
HKMD under 200 kPa
40°C
Cooling-20°C
Prediction by TEVP
t_e+t_0
1.E+10
1.E+08
1.E+06
1.E+04
1.E+02
$t_e + t_0$ (min)

Fig. 16c

Click here to access/download;Figure;Fig 16c.pdf

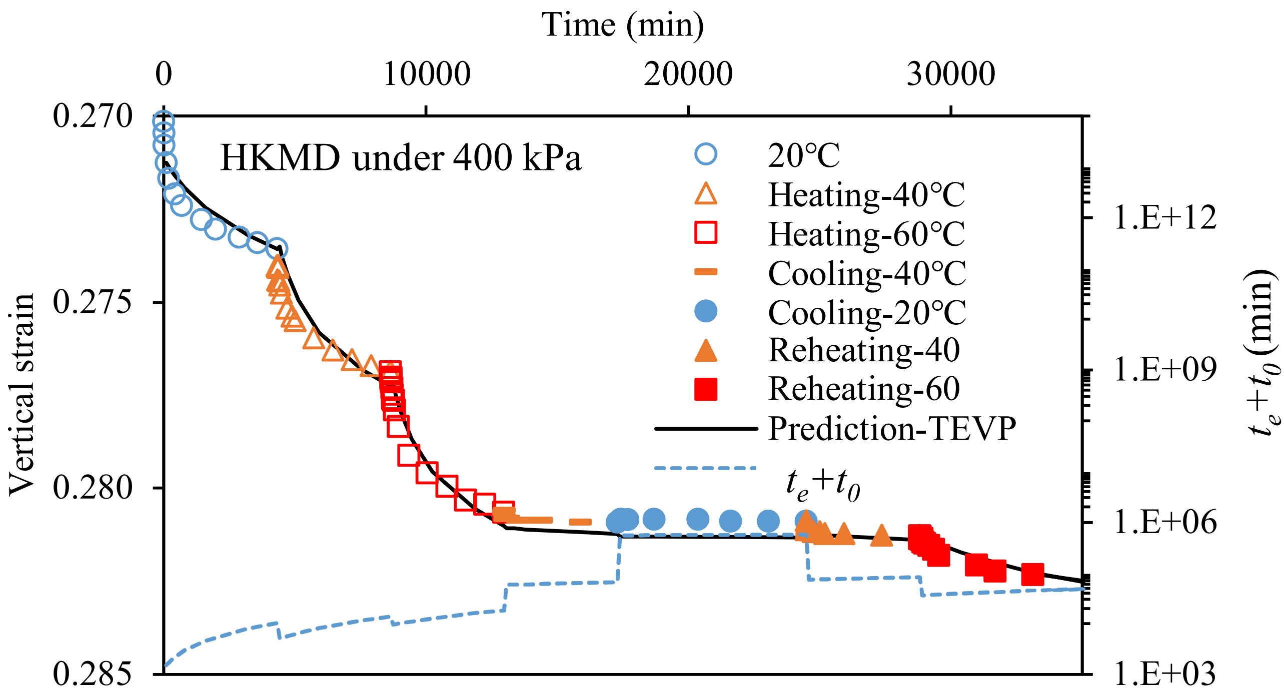

Fig. 16d

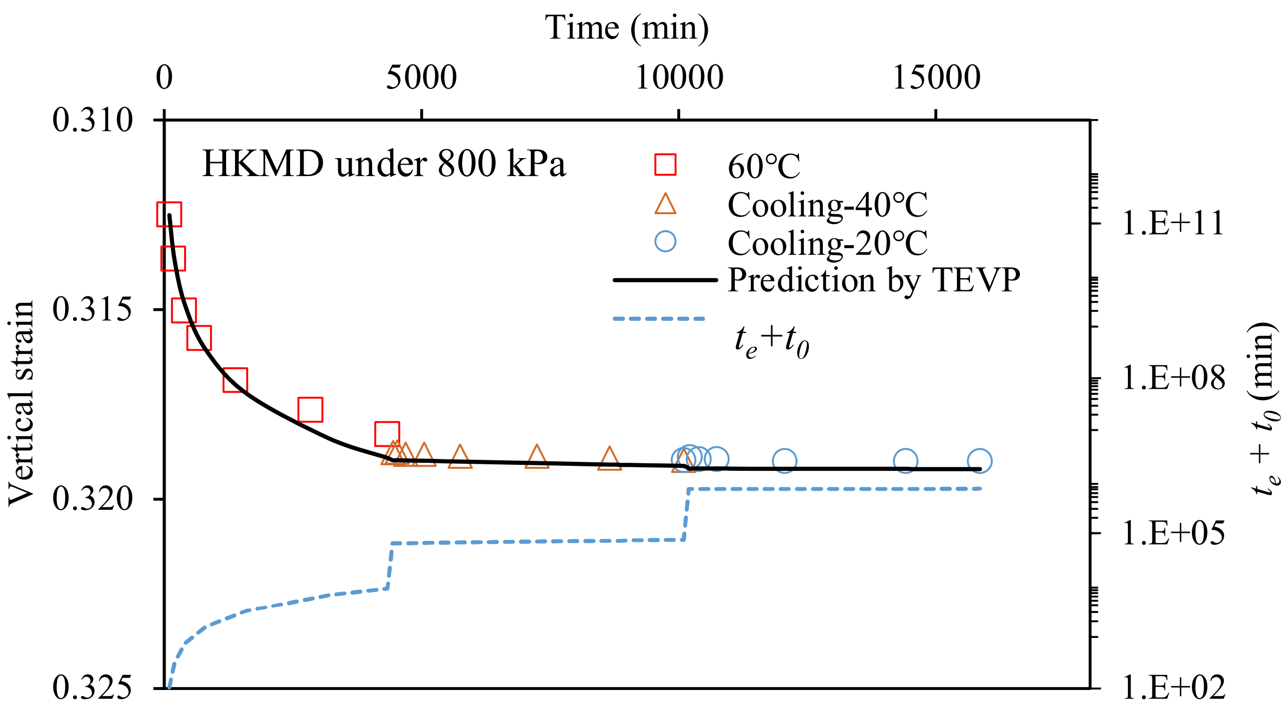
Time (min)
0
5000
10000
15000
0.310
0.315
0.320
0.325
Vertical strain
HKMD under 800 kPa
60℃
Cooling-40℃
Cooling-20℃
Prediction by TEVP
$t_e + t_0$
1.E+11
1.E+08
1.E+05
1.E+02
$t_e + t_0$ (min)

Fig. 16e

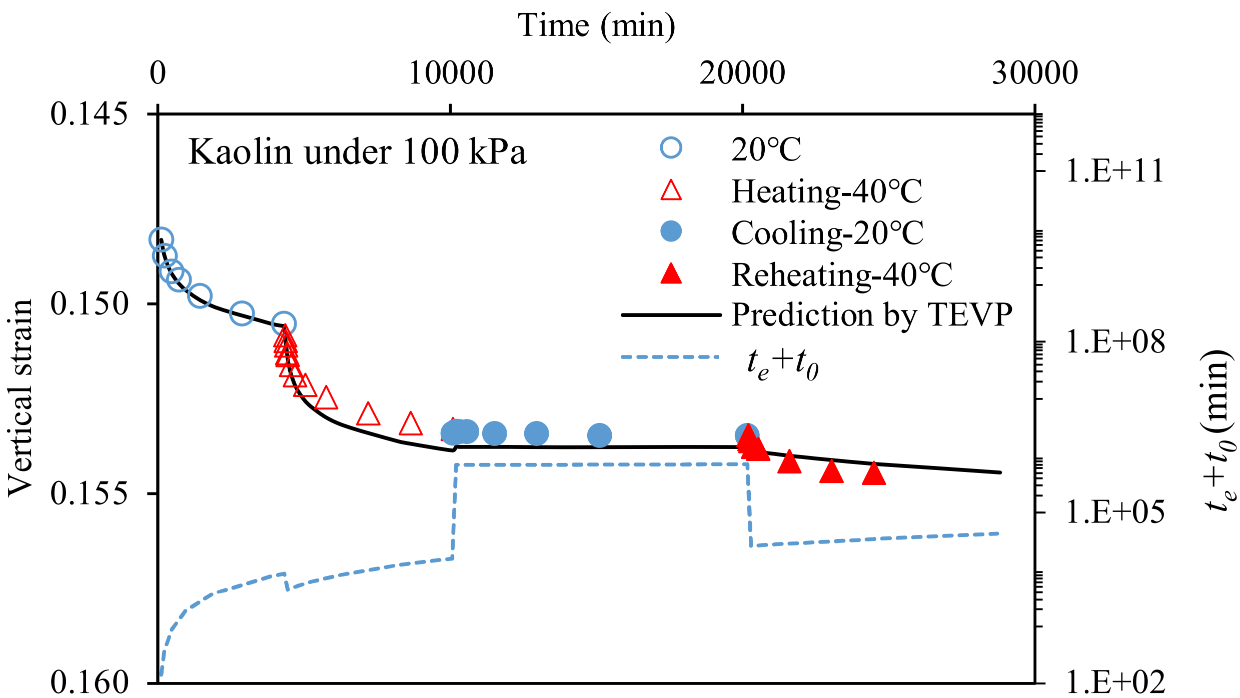

Time (min)
0
10000
20000
30000
0.145
0.150
0.155
0.160
Vertical strain
1.E+11
1.E+08
1.E+05
1.E+02
t_e+t_0 (min)
Kaolin under 100 kPa
20°C
Heating-40°C
Cooling-20°C
Reheating-40°C
Prediction by TEVP
t_e+t_0

Fig. 16f

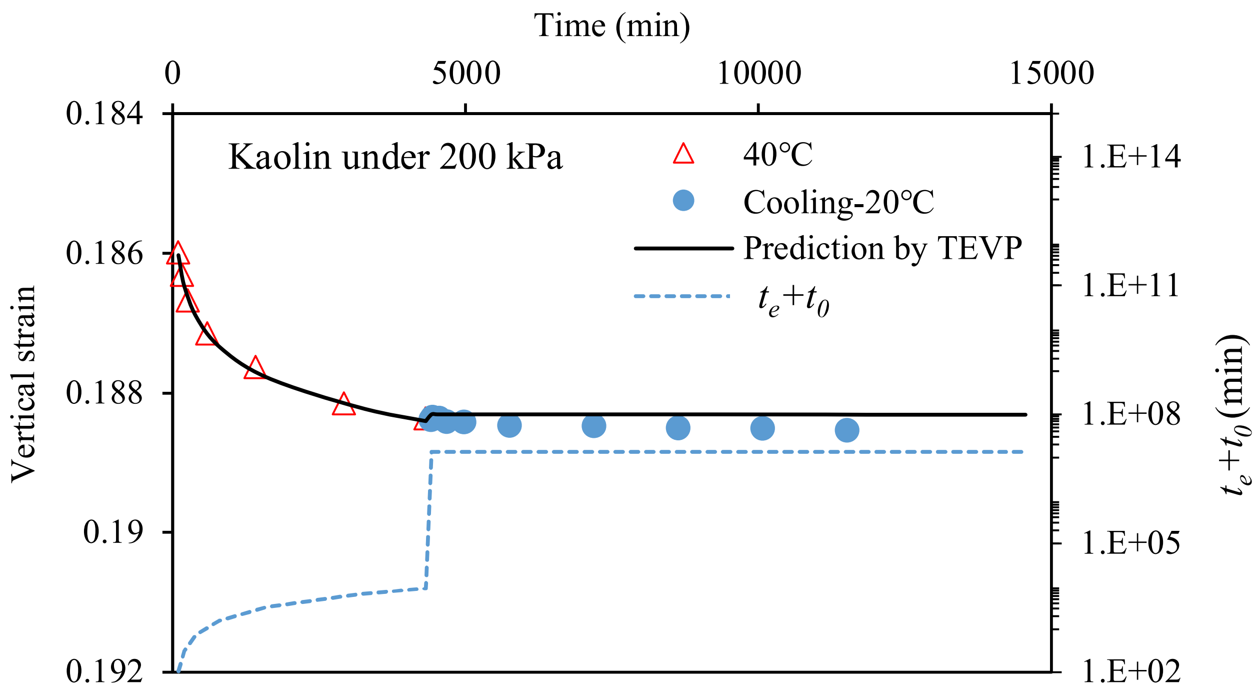

Time (min)
0
5000
10000
15000
0.184
0.186
0.188
0.19
0.192
Vertical strain
Kaolin under 200 kPa
40°C
Cooling-20°C
Prediction by TEVP
t_e+t_0
1.E+14
1.E+11
1.E+08
1.E+05
1.E+02
t_e+t_0 (min)

Fig. 16g

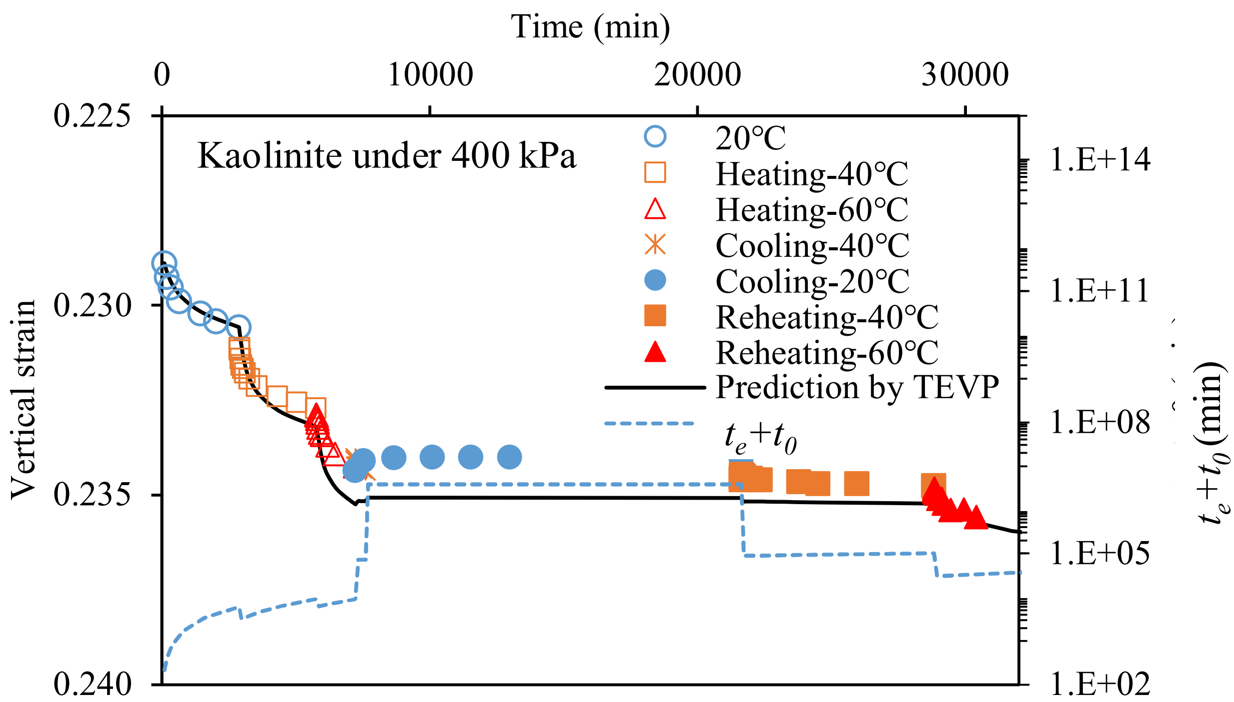

Time (min)
0
10000
20000
30000
0.225
0.230
0.235
0.240
Vertical strain
Kaolinite under 400 kPa
20℃
Heating-40℃
Heating-60℃
Cooling-40℃
Cooling-20℃
Reheating-40℃
Reheating-60℃
Prediction by TEVP
t_e+t_0
1.E+14
1.E+11
1.E+08
1.E+05
1.E+02
t_e+t_0 (min)

Fig. 16h

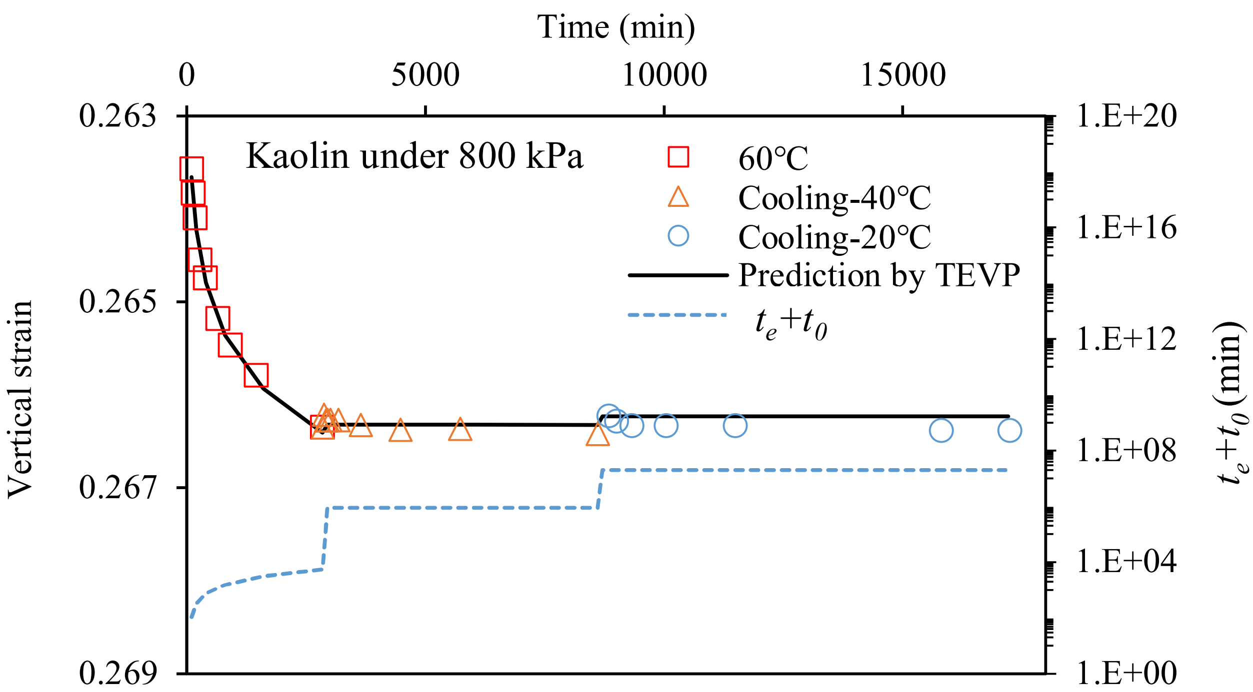
Time (min)
0
5000
10000
15000
0.263
0.265
0.267
0.269
Vertical strain
1.E+20
1.E+16
1.E+12
1.E+08
1.E+04
1.E+00
t_e+t_0 (min)
Kaolin under 800 kPa
60°C
Cooling-40°C
Cooling-20°C
Prediction by TEVP
t_e+t_0

Figure Captions

Fig.1. Test setup of the temperature-controlled oedometer

Fig.2. Calibration results for the temperature-controlled oedometer: (a) temperature distribution inside the soil; (b) temperature with time

Fig.3. Particle size distribution curves of HKMD and kaolin

Fig.4. Typical $\varepsilon_z - \log(t)$ curves under loading and heating in oedometer (HKMD under 100 kPa)

Fig.5. Measured relations of vertical strain and time under changes of temperature: (a) HKMD under 100 kPa; (b) HKMD under 400 kPa; (c) kaolin under 100 kPa; (d) kaolin under 400 kPa

Fig.6. Measured relations of vertical strain and temperature: (a) HKMD under 100 kPa; (b) HKMD under 400 kPa; (c) kaolin under 100 kPa; (d) kaolin under 400 kPa

Fig.7. Illustration for the calculation of creep strain rate $\dot{\varepsilon}_z^{vp}$ with the oedometer test data

Fig.8. Measured relations between creep strain rate $\dot{\varepsilon}_z^{vp}$ and vertical strain ε_z under different temperatures: (a) HKMD under 100 kPa; (b) HKMD under 400 kPa; (c) kaolin under 100 kPa; (d) kaolin under 400 kPa

Fig.9. 1D compression curves for: (a) HKMD and kaolin (at t_0); (b) natural Bangkok clay (after Abuel-Naga et al. 2006) and HK clay

Fig.10. A schematic diagram for modelling the effect of temperature under constant effective vertical stress

Fig.11. A schematic diagram on incorporating temperature into 1D EVP model

Fig.12. A schematic graph indicating the stress–temperature–strain relationship in TEVP model

Fig.13. The thermal induced strain of kaolin under 1600 kPa with three incremental temperature loadings (20 °C, 40 °C and 60 °C): (a) vertical strain with log(time); (b) vertical strain with different temperatures (at t_0 unless otherwise stated)

Fig.14. Illustration of the second method for calculating $\frac{\lambda_T}{V}$ with $\ln\dot{\varepsilon}_z^{vp} - \varepsilon_z$ data

Fig.15. Measured relations between temperature and strain of over-consolidated HKMD under different OCR (at t_0 unless otherwise stated)

Fig.16. Predictions of 1D creep strain under changes of temperature by TEVP with comparisons to experimental data: (a) HKMD under 100 kPa; (b) HKMD under 200 kPa; (c) HKMD under 400 kPa; (d) HKMD under 800 kPa; (e) kaolin under 100 kPa (e) kaolin under 200 kPa; (g) kaolin under 400 kPa; (h) kaolin under 800 kPa